

Chemical optimization of siRNA for safe and efficient silencing of placental sFLT1

Sarah M. Davis,^{1,7} Vignesh N. Hariharan,^{1,7} Agnes Lo,^{2,3,7} Anton A. Turanov,¹ Dimas Echeverria,¹ Jacquelyn Sousa,¹ Nicholas McHugh,¹ Annabelle Biscans,¹ Julia F. Alterman,¹ S. Ananth Karumanchi,^{2,3,4} Melissa J. Moore,^{1,5} and Anastasia Khvorova^{1,6}

¹RNA Therapeutics Institute, University of Massachusetts Medical School, AS4-1049, 368 Plantation Street, Worcester, MA 01605, USA; ²Center for Vascular Biology Research, Beth Israel Deaconess Medical Center, Boston, MA, USA; ³Harvard Medical School, Boston, MA, USA; ⁴Department of Medicine, Cedars-Sinai Medical Center, Los Angeles, CA, USA; ⁵Moderna Therapeutics, Cambridge, MA, USA; ⁶Department of Molecular Medicine, University of Massachusetts Medical School, AS4-1049, 368 Plantation Street, Worcester, MA 01605, USA

Preeclampsia (PE) is a rising, potentially lethal complication of pregnancy. PE is driven primarily by the overexpression of placental soluble fms-like tyrosine kinase 1 (sFLT1), a validated diagnostic and prognostic marker of the disease when normalized to placental growth factor (PlGF) levels. Injecting cholesterol-conjugated, fully modified, small interfering RNAs (siRNAs) targeting *sFLT1* mRNA into pregnant mice or baboons reduces placental sFLT1 and ameliorates clinical signs of PE, providing a strong foundation for the development of a PE therapeutic. siRNA delivery, potency, and safety are dictated by conjugate chemistry, siRNA duplex structure, and chemical modification pattern. Here, we systematically evaluate these parameters and demonstrate that increasing 2'-O-methyl modifications and 5' chemical stabilization and using sequence-specific duplex asymmetry and a phosphocholine-docosanoic acid conjugate enhance placental accumulation, silencing efficiency and safety of *sFLT1*-targeting siRNAs. The optimization strategy here provides a framework for the chemical optimization of siRNAs for PE as well as other targets and clinical indications.

INTRODUCTION

Preeclampsia (PE) affects up to 10% of human pregnancies worldwide,¹ and is a leading cause of maternal and fetal mortality and morbidity. Women with PE develop hypertension, often with proteinuria, after 20 weeks of pregnancy. Maternal complications include kidney failure, pulmonary edema, and stroke. PE also increases adverse outcomes for the baby, including mortality, growth restriction, cerebral palsy, and cardiovascular disease in adulthood. Delivery is currently the only curative treatment for PE, but it can cause preterm birth complications and adverse clinical outcomes, depending on gestational age.^{1–4}

Although the etiology and pathophysiology of PE are unclear, high serum levels of soluble fms-like tyrosine kinase 1 (sFLT1) is a major contributor to the clinical signs of the disease and is directly linked to disease severity.^{5–11} sFLT1 variants result from alternative polyadenylation of vascular endothelial growth factor receptor 1 (VEGFR1) and include the extracellular domain of VEGFR1. When secreted from

placenta, sFLT1 variants sequester VEGF and placental growth factors circulating in the blood.^{12,13} Exogenous VEGF supplementation or reduction of sFLT1 improve PE symptoms in humans and animal models.^{6,14–18}

Small interfering RNA (siRNA) is a promising class of drugs that bind complementary, target mRNA to reduce its expression.¹⁹ We previously found that siRNA targeting the most highly upregulated sFLT1 mRNA variants in PE placenta²⁰ (i.e., *sFLT1-i13* [short], *sFLT1-i13* [long], and *sFLT1-e15a*) selectively reduce placental *sFLT1* mRNA and circulating serum sFLT1 protein in mice and circulating serum sFLT1 protein, blood pressure, and proteinuria in baboons.²¹ These asymmetric siRNA were conjugated to cholesterol (Chol) and used 2'-O-methyl (2'-OMe) and 2'-fluoro (2'-F) ribose modifications in an alternating pattern,²² terminal phosphorothioate (PS) linkages, and a phosphate at the 5' end of the antisense (or “guide”) strand of the siRNA, which facilitates recognition by the siRNA effector protein Argonaute 2 (Ago2) (Figure 1). Owing to continued advances in siRNA chemistries, this early-generation scaffold could be further optimized.

Chol conjugation delivers siRNA to a wide range of tissues, especially those that are highly vascular with fenestrated endothelia, like placenta.^{23–27} However, Chol-conjugated siRNAs can cause cytotoxicity at higher doses with significant acute cytokine stimulation compared to other hydrophobic conjugates.^{28–30} In addition to the hydrophobic conjugate, the chemical structure of the siRNA backbone, such as duplex symmetry,³¹ PS content,³² and the number and position of 2'-OMe modifications,³³ affect siRNA distribution, potency, and safety. Indeed, the most clinically advanced siRNAs, which are conjugated to *N*-acetyl-galactosamine (GalNac) for liver-specific delivery, require 5' PS

Received 5 January 2022; accepted 15 June 2022;
<https://doi.org/10.1016/j.omtn.2022.06.009>.

⁷These authors contributed equally

Correspondence: Anastasia Khvorova, PhD, University of Massachusetts Medical School, RNA Therapeutics Institute, AS4-1049, 368 Plantation Street, Worcester, MA 01605, USA.

E-mail: anastasia.khvorova@umassmed.edu



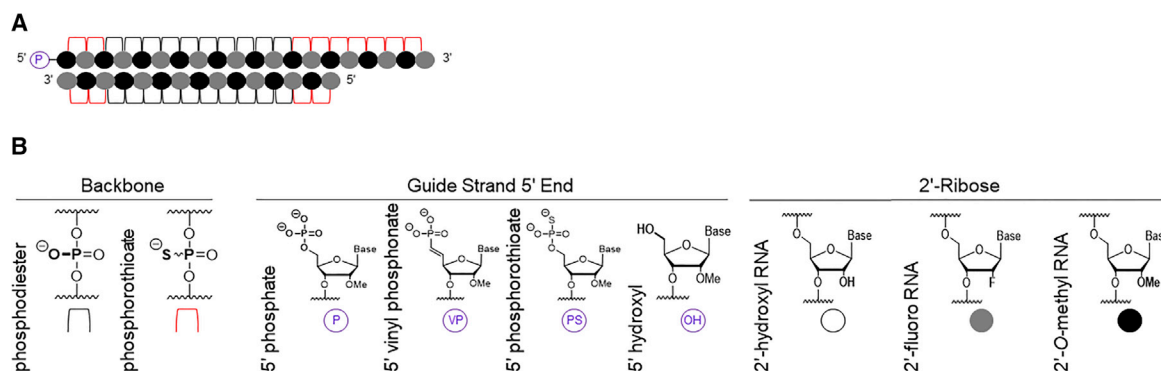


Figure 1. siRNA chemical modifications used in this study

(A) Schematic of asymmetric siRNA with alternating 2'-OMe/2'-F chemical pattern. (B) Corresponding chemical modifications.

modifications for exonuclease stability³⁴ and increased 2'-OMe content for increased metabolic stability³³ to achieve safe, efficacious, and sustained (>6 months) gene modulation *in vivo*.³⁵ Further modification of the guide strand with the stable analog 5'-(E)-vinylphosphonate (VP) may also improve potency and stability *in vivo*.^{36–38}

Here, we show how sequential modifications of chemical architecture, including hydrophobic conjugate, duplex symmetry, 2'-OMe content, and 5' moiety, optimize the placental delivery, silencing efficiency, and safety of *sFLT1*-targeting siRNAs. This work outlines an approach for the systematic evaluation of siRNA chemical parameters for the optimization of these characteristics.

RESULTS

PC-DCA conjugation increases siRNA accumulation in mouse placenta

We found that *sFLT1*-targeting Chol-siRNAs efficiently deliver to placenta with primary liver clearance.²¹ Changing the chemical conjugate alters tissue distribution profiles and silencing efficiency of siRNA in non-pregnant mice,^{32,39} but the effect of conjugate modality on placental accumulation has not been determined.

To explore whether changing conjugate modality could enhance placental accumulation, we synthesized a panel of fully modified Huntingtin (*Htt*) targeting siRNAs conjugated to Chol, docosahexaenoic acid (DHA, 22:6 n-3), or docosanoic acid (DCA, 22:0) with or without the polar head group, phosphatidylcholine (PC) (siRNA 1–5). All of the conjugates were attached to the sense strand via a phosphodiester bond. These conjugates previously demonstrated delivery to a wide range of tissues.³⁰ Divalent (DIO) (siRNA 6) and non-conjugated (NOC) siRNAs were used to control for the relative contribution of conjugate and compound size to distribution. DIO siRNA contains 2 passenger strands covalently connected at their 3' ends through a tetra-ethylene glycol linker base paired to two identical guide strands. DIO and conjugated siRNA structures are shown in Figures 2A and 2B (chemical modification legend in Figure 1A). The same sequence was used for all of the compounds; this sequence and all of the modification patterns are shown in Table S1.

Pregnant CD1 mice were subcutaneously injected with 20 mg/kg *Htt*-targeting siRNA (n = 3 mice/group) and sacrificed after 48 h. We used 2 complementary assays to evaluate siRNA tissue accumulation. First, we attached a Cy3 fluorophore to the 5' end of the siRNA passenger strand. Cy3 has minimal impact on hydrophobic siRNA tissue distribution,³⁰ and enables the qualitative evaluation of spatial distribution in organs (Figure 2C). Second, we used peptide nucleic acid (PNA) hybridization, which enables quantification of the guide strand (Figure 2D).⁴⁰ PNA hybridization does not rely on the presence of Cy3 on siRNA and thus can be used for the quantification of labeled or non-labeled compounds.

NOC siRNA showed essentially no placental accumulation; most of the injected compound was retained in and cleared by the kidney. The DIO siRNA, which shows promising results for CNS delivery,³⁹ reduced renal retention but did not support appreciable accumulation in placenta (Figures 2C and 2D). Consistent with previous studies, Chol siRNA, DCA siRNA, and PC-DCA siRNA showed higher accumulation in liver and lower accumulation in kidney relative to DHA siRNA, PC-DHA siRNA, and NOC siRNAs. This is because less hydrophobic compounds (i.e., DHA and PC-DHA) preferentially bind high-density lipoproteins that traffic to kidney, while more hydrophobic compounds (i.e., Chol, DCA, and PC-DCA) preferentially bind low-density lipoproteins, which traffic to liver.^{24,30}

PC-DCA siRNAs showed the highest accumulation in placenta compared to the other chemistries, including Chol (Figures 2C, 2D, and S1C). Because conjugate-mediated siRNA delivery is defined by conjugate chemistry, not the sequence,^{30,32} data generated for one sequence can in most cases be used to predict the behavior of other siRNA with similar conjugate chemistry. PC-DCA was therefore selected as the best conjugate for siRNA-mediated downregulation of placental *sFLT1*.

The impact of siRNA duplex asymmetry on *sFLT1*-targeting siRNA activity

A 20-nt/15-nt structure was used for *sFLT1*-targeting siRNA in our previous study.²¹ Separately, we demonstrated that the presence and

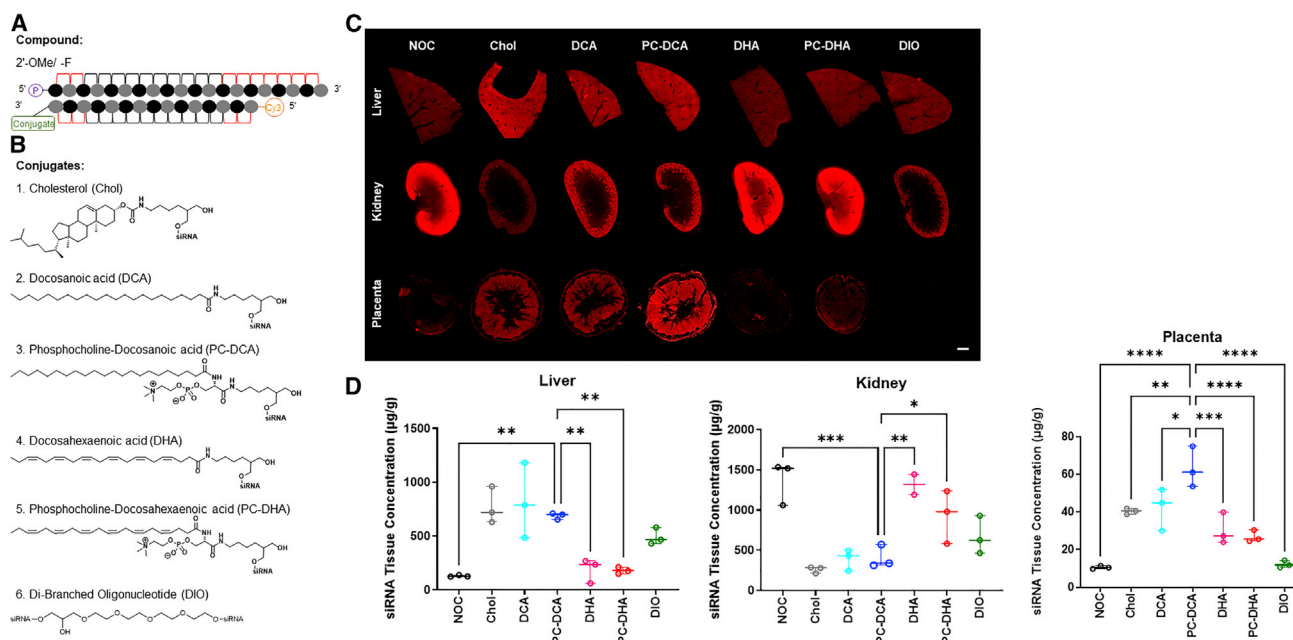


Figure 2. PC-DCA siRNA conjugates demonstrate enhanced placental accumulation

Pregnant CD1 mice subcutaneously injected with 20 mg/kg Cy3 labeled siRNA variants on embryonic day (E) 14. (A) Schematic of chemical modification scaffold used. (B) Chemical structure of siRNA conjugates. (C) Tissue fluorescence imaging. Leica DM5500. 10× tiled array images. Scale bar, 1 mm. All images acquired at identical laser intensity. NOC, no conjugate. (D) Guide strand accumulation quantified after 48 h by PNA hybridization assay; n = 3 mice/group; average results shown from 3 liver or kidney punches/mouse or 6 placenta/mouse (1 punch/placenta). p values describe statistically significant differences between each compound and the PC-DCA compound (1-way ANOVA; *p < 0.05, **p < 0.01; ***p < 0.001; ****p < 0.0001; non-significant differences unmarked).

length of PS-modified single-stranded overhangs at the 3' end of the siRNA guide strand significantly affect silencing efficiency in a sequence-specific manner.³² To systematically evaluate the impact of duplex asymmetry/overhang length on the activity of *sFLT1*-targeting siRNA, we created a panel of compounds with different lengths of 3' guide strand overhangs. Overhangs were created by varying lengths of the passenger strand from 12 to 20 nt (Figures 3A and 3B; Table S2). Two sequences were used, *sFLT1-i13_2283* and *sFLT-e15a_2519*, which target the *sFLT1-i13* (siRNA 8–14) and *sFLT1-e15a* (siRNA 15–21) isoforms, respectively.²¹ The siRNA panel was tested in HeLa cells using a Dual-Glo Luciferase reporter (see Materials and methods). Each siRNA was evaluated by a 7-point dose-response curve (Figures 3C and 3D).

For both siRNA sequences, the 12-nt passenger strand (siRNA 8 and 15) was inactive, indicating a lower limit to passenger strand length that can support RNAi activity. This is similar to what has been reported.⁴¹ In the case of *sFLT1-i13_2283*, passenger strand lengths of 14 nt and above were tolerated (siRNA 10–14), with the 14-nt strand (siRNA 10) supporting the highest activity (Figure 3C). Elimination of duplex asymmetry with the 20-nt passenger strand (siRNA 14) negatively affected silencing. In the case of *sFLT-e15a_2519*, a passenger strand length of at least 16-nt (siRNA 19 and 20) was required for maximal activity. Elimination of asymmetry (siRNA 21) did not negatively affect activity (Figure 3D).

To explore whether we could further improve the activity of siRNAs with either the 14-nt or 16-nt passenger strand, we applied chemical modifications (shown in Figure S2B) that are thought to decrease duplex stability and encourage duplex unwinding, the mechanism used to release the passenger strand following duplex loading onto Ago2 (Figure S2; Table S2).⁴² In 14-nt passenger strands, 2'-F was replaced with 2'-OMe at positions 2 and 14 (across from guide strand positions 13 and 1 because 2'-OMe confers looser base stacking interactions than 2'-F.⁴³ In 16-nt strands, we substituted cytosine (C) for adenine (A) at position 8 (i.e., across from 2'-OMe guide strand position 9) to introduce a bulge in the duplex.⁴⁴ We found neither strategy to be effective. siRNA activity was minimally affected by the new 14-nt strand and severely inhibited by the mismatch in the 16-nt strand (Figures S2C and S2D).

Chemical pattern affects activity of *sFLT1*-targeting siRNAs

In parallel to testing the impact of duplex asymmetry on siRNA activity, we tested the impact of varying 2'-OMe/2'-F modification patterns on siRNA activity using the same methods. Guide strands (Figure S3A) were designed to include a (1) 3' terminal 2'-OMe (position 20), to enhance exonuclease stability;⁴⁵ (2) 2'-F at positions 5 and 7, to increase target affinity for the siRNA seed (i.e., guide strand positions 2–8); and (3) an additional 2'-OMe at positions 12, 16, or 18, to enhance guide strand stability. Position 14 was maintained as 2' F due to the well-reported limited tolerance of 2'-OMe at this position.^{33,46,47} The guide strand panel was evaluated in the context of

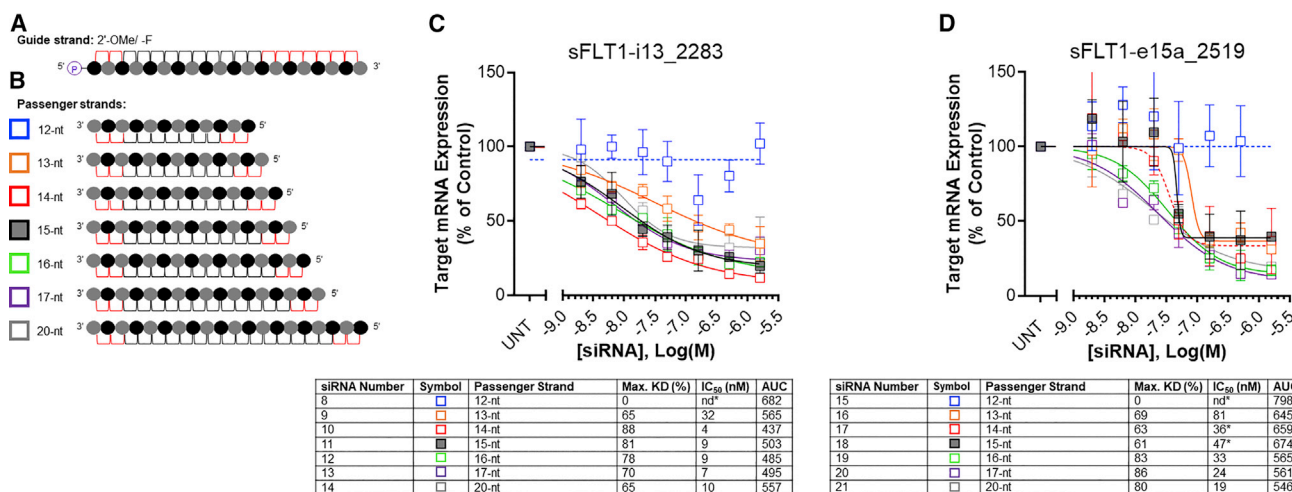


Figure 3. Impact of passenger strand length on compound activity varies for each siRNA sequence

(A) Schematic of guide strand chemical modification pattern. (B) Schematic of cholesterol-conjugated passenger strand chemical modification patterns; symbols next to each schematic used in graphs. (C and D) Dose-response results ($n = 3$, means \pm SDs). Target name and start site of target sequence indicated in each graph. HeLa cells treated with siRNAs at concentrations shown for 72 h. mRNA levels measured using the Dual-Glo Luciferase Assay System and calculated as percentage of untreated control. Non-linear regression curves with $R^2 < 0.8$ displayed as dashed lines. Each table reports values corresponding to graph: Maximum K_D (%), maximum percentage target mRNA knockdown with top treatment dose of siRNA; IC_{50} , half maximal inhibitory concentration ($R^2 < 0.8$; nd, not determined); AUC, area under the dose-response curve.

2 different 15-nt passenger strands, one having the conventional alternating 2'-OMe/2'-F composition (siRNA 26–41) and the other containing 80% 2'-OMe content (siRNA 42–57) to see whether high 2'-OMe content in the passenger strand could be tolerated (Figure S3B; Table S2).

As previously reported,⁴⁸ 2'-OMe at guide strand position 20 negatively affected activity (siRNA 27, 35, 43, and 51); however, the addition of 2'-F at position 5 (siRNA 29, 37, 45, and 53), and to a lesser extent at position 7 (siRNA #32, 40, 48, and 56), had a partial compensatory effect (Figures S3C and S3D). Interestingly, for some variants, pairing the guide strand with the 80% 2'-OMe passenger strand improved the area under the curve (AUC) compared to pairing with the alternating 2'-OMe/F passenger strand (siRNA 29 versus 45, 37 versus 53, 30 versus 46, 38 versus 54, 39 versus 55) (Figures S3E and S3F). The AUC metric was used in cases in which the dose-response curve was incomplete (i.e., zero knockdown or maximum knockdown was not achieved in the dose range tested). Incomplete dose-response curves result in unreliable half-maximal inhibitory concentration (IC_{50}) values, while AUC is a versatile metric that can be used on any kind of dose-response curve.⁴⁹ This result suggests that increasing 2'-OMe content of the guide strand in certain positions needs corresponding increases in 2'-OMe in the passenger strand to retain siRNA activity.

sFLT1-targeting siRNAs can tolerate 2'-OMe-rich chemical modification patterns

Since increasing 2'-OMe modifications in the guide strand was better tolerated when paired with 2'-OMe-rich passenger strands, we tested various 2'-OMe-rich patterns in the guide strand in the context of a fully 2'-OMe passenger strand (siRNA 58–61) (Figure 4A; Table S2). These 2'-OMe-rich duplexes ranged from 83% to 94%

2'-OMe content, and were tested alongside the conventional alternating 2'-OMe/2'-F control siRNA (siRNA 26 and 34) and the best performing variant from the previous experiment (siRNA 45 and 53 in Figure S3), which had an overall 2'-OMe content of 63%. The activity of sFLT1-i13_2283 was minimally perturbed in the context of 86% 2'-OMe content (siRNA 58) but increasing 2'-OMe content to 94% (siRNA 59) was less tolerated (Figure 4B). In the context of sFLT1-e15a_2519, all 2'-OMe-rich variants improved activity compared to the 2'-OMe/2'-F modification pattern (Figure 4C).

To confirm the silencing efficiency of selected scaffolds in the context of endogenous mRNA, we tested the high 2'-OMe-rich scaffolds in WM-115 human melanoma cells using the sFLT1 QuantiGene assay (see Materials and methods). The 2'-OMe-rich scaffolds retained siRNA activity and did not differ from conventional 2'-OMe/2'-F control siRNA activity for both sFLT1-i13_2283 and sFLT1-e15a_2519 (Figures 4D and 4E). Thus, in the context of endogenous mRNA, 2'-OMe-rich siRNA can efficiently load into Ago2 and silence sFLT1. Since an increase in 2'-OMe content is expected to significantly enhance overall stability and activity *in vivo*,^{33,50,51} we chose siRNA 58 (86% 2'-OMe, Figure 4D) as the scaffold for sFLT1-i13_2283 and siRNA 61 (94% 2'-OMe, Figure 4E) as the scaffold for sFLT1-e15a_2519 for further analyses.

These patterns were combined with the optimized duplex asymmetry identified (i.e., 14-nt passenger strand for sFLT1-i13_2283 and 16-nt passenger strand for sFLT1-e15a_2519) (from Figures 3C and 3D) and the PC-DCA conjugate for *in vivo* testing. In the case of sFLT1-e15a_2519, 16-, 17-, and 20-nt passenger strands showed only minimal differences in potency. The configuration providing maximum asymmetry (i.e., 16-nt) was selected because asymmetry

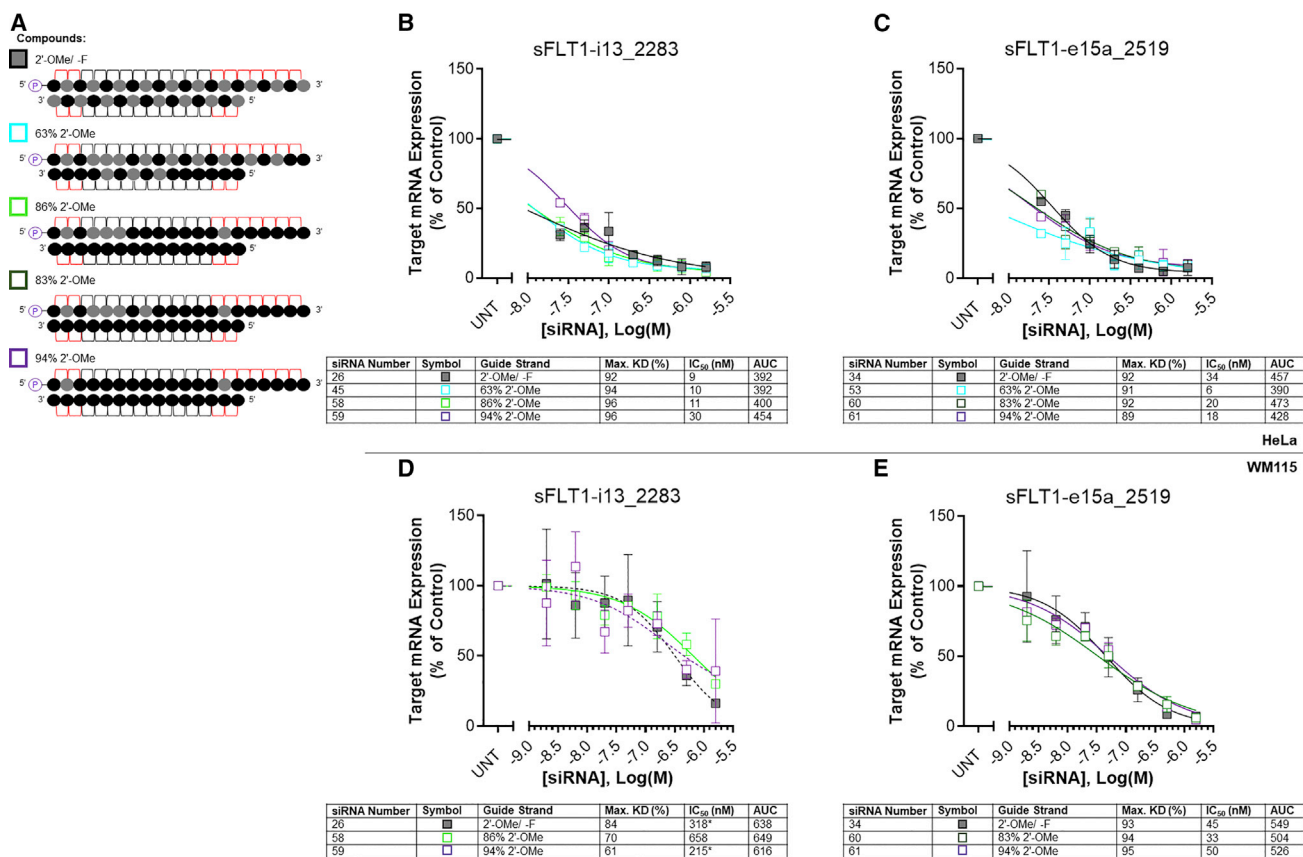


Figure 4. 2'-OMe-rich chemical modification patterns do not significantly reduce silencing

(A) Schematic of cholesterol conjugated compounds; symbols next to each schematic used in graphs. (B–E) Dose-response results ($n = 3$, means \pm SDs). Target name and start site of target sequence indicated in each graph. HeLa or WM115 cells treated with siRNAs at concentrations shown for 72 h. mRNA levels measured using the Dual-Glo Luciferase Assay System (HeLa) or Quantigene 2.0 RNA Assay (WM-115) and calculated as a percentage of untreated control. Non-linear regression curves with $R^2 < 0.8$ displayed as dashed lines. Each table reports values corresponding to graph: Maximum KD (%), maximum percentage target mRNA knockdown with top treatment dose of siRNA, IC₅₀, half-maximal inhibitory concentration ($*R^2 < 0.8$, and nd, not determined); AUC, area under the dose-response curve.

has been shown to be beneficial for *in vivo* activity compared to blunt siRNAs.³²

Optimization of siRNA 5' moiety improves placental accumulation and silencing

The 5' chemical moiety on the guide strand anchors it to the MID domain of Ago2 during siRNA loading.^{52,53} For many siRNA sequences, the presence of a 5'-phosphate improves MID domain binding.^{53,54} Incorporation of a more stable phosphate mimic, VP, may further improve siRNA stability and silencing efficiency.^{37,38,55–57} We tested the impact of 5'-VP (siRNA 62 and 65), 5'-OH (siRNA 63 and 66), or 5'-PS (siRNA 64 and 67) on placental accumulation and silencing efficiency of PC-DCA-conjugated siRNA in the optimized asymmetric, 2'-OMe-rich scaffold (Figures 5A and 5B; Table S1). The *sFLT1-e15a* isoform is expressed only in humans and non-human primates; thus, *in vivo* activity of sFLT1-e15a_2519 cannot be assessed in mice. Nevertheless, to maintain consistency with future studies in humans and non-human primates, a 1:1 mixture of both compounds, sFLT1-i13_2283 and sFLT1-

e15a_2519, were injected into mice for evaluation. The non-targeting control (NTC) similarly consisted of a 1:1 mixture of a non-targeting sequence synthesized in each optimized scaffold. The silencing efficiency data shown in Figure 5 corresponds to the activity of sFLT1-i13_2283 since that is the only target expressed in mice.

Both 5'-OH and 5'-PS variants silenced *sFLT1-i13* by 47%–48% ($p < 0.0001$). We observed a small but significant improvement in silencing by 5'-VP-containing siRNA compared to 5'-OH and 5'-PS (66%, $p < 0.01$; Figure 5C). In addition to enhanced silencing efficiency, 5'-VP compounds showed higher placental levels compared to 5'-OH compounds (_2283: 44 μ g/g versus 31 μ g/g, $p < 0.01$; _2519: ~80 μ g/g versus 63 μ g/g; Figure 5D). Therefore, we elected to incorporate 5'-VP into our optimized scaffold.

The PC-DCA conjugate reduces monocyte saturation, the primary cause of dose-limiting toxicity

Unlike unmodified RNAs, which activate Toll-like receptors (TLRs) and the inflammatory cytokine-driven immune response,^{58,59} fully

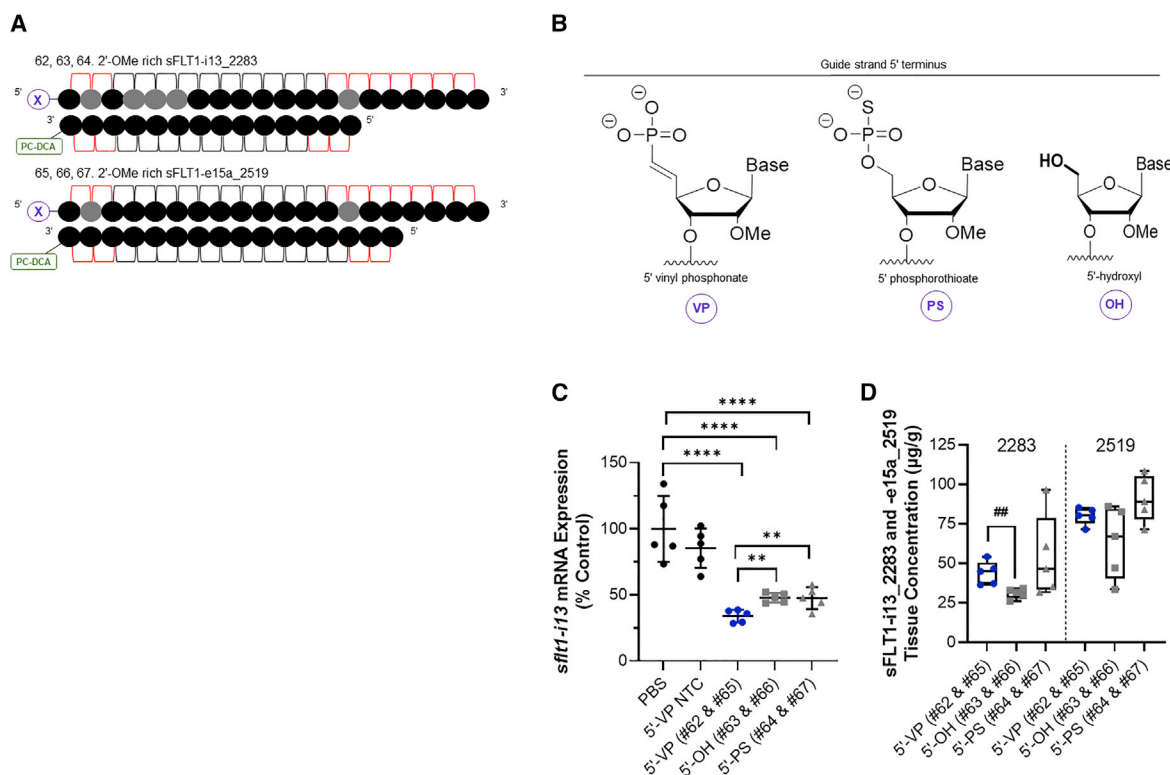


Figure 5. Optimization of 5'-moiety results in increased tissue accumulation and silencing efficiency *in vivo*

Pregnant CD1 mice injected with a mixture of 20 mg/kg sFLT1-i13_2283 and 20 mg/kg sFLT1-e15a_2519 siRNA variants on E13 and E14. (A) Schematic of the chemical pattern of siRNA compounds injected. (B) Chemical structures of 5'-moieties tested. (C) *sft1-i13* mRNA levels in placenta on E18 measured using the Quantigene 2.0 RNA Assay. Levels were normalized to *Flt1* and presented as a percentage of PBS control (n = 5, means ± SDs). (D) Amount of siRNA accumulation in the placenta on E18 measured using PNA hybridization assay (n = 5). p values describe statistically significant differences between compounds (1-way ANOVA; **p < 0.01; ****p < 0.0001. Unpaired t test; ##p < 0.01. Non-significant differences unmarked).

2'-F or 2'-OMe modified siRNAs are non-inflammatory and, in certain contexts, antagonistic to TLR stimulation.^{60–65} However, Chol conjugation to fully modified siRNA induces a cytokine response at higher doses,^{28–30} possibly due to its accumulation in the immune cells of bone marrow that play a role in the cytokine response of the innate immune system. PE itself is associated with immune imbalances and chronic inflammation, which sets up a cycle of oxidative damage that promotes further oxidative stress.^{66,67} Thus, if not carefully optimized, the innate immune stimulatory potential of Chol-siRNAs may negate the therapeutic benefit of sFLT1 reduction. We decided to test the immune stimulatory potential of and acute cytokine response to PC-DCA versus Chol siRNA in the optimized 2'-OMe-rich, asymmetric, 5'-VP scaffold.

We used fluorescence-activated cell sorting (FACS) to measure accumulation of Cy3-labeled conjugated siRNA in immune cell populations of bone marrow. Since the exact cell populations that may be involved in the immune response to fully modified siRNA are unclear, we chose a cell staining and gating strategy that provided us with broad cell populations. For this experiment, granulocytes and monocytes were chosen as broad innate immune cell categories. In addition

to granulocytes and monocytes, a granulocyte subpopulation consisting primarily of neutrophils was studied since these are the most predominant granulocytes in circulation and are often involved in initiating an immune response.⁶⁸

Cy3-labeled sFLT-i13_2283 with either the Chol (siRNA 68) or PC-DCA (siRNA 69) conjugate (Figure 6A; Table S1) were injected at three different doses in non-pregnant mice. Femur bone marrow cells were sorted 24 h post-injection and gated to identify immune cell populations as follows: First, singlet cells were identified by plotting forward scatter area (FSC-A) versus forward scatter height (FSC-H) and selecting cells along the diagonal through the origin (Figure 6B, top left scatterplot). The singlets were then visualized on a graph of granularity (side scatter, SSC-A) versus size (FSC-A) to exclude lymphocyte populations and select potential monocytes (lower gate) and granulocytes (upper gate) (Figure 6B, middle scatterplot). Monocytes were defined as the CD11b⁺ population of the lower gate (Figure 6B, bottom scatterplot). Neutrophils, broadly defined as Gr-1⁺ high granulocytes, were selected from a graph of granularity (SSC-A) versus Gr-1 staining intensity (Figure 6B, top right scatterplot). Fraction and intensity of Cy3-labeled

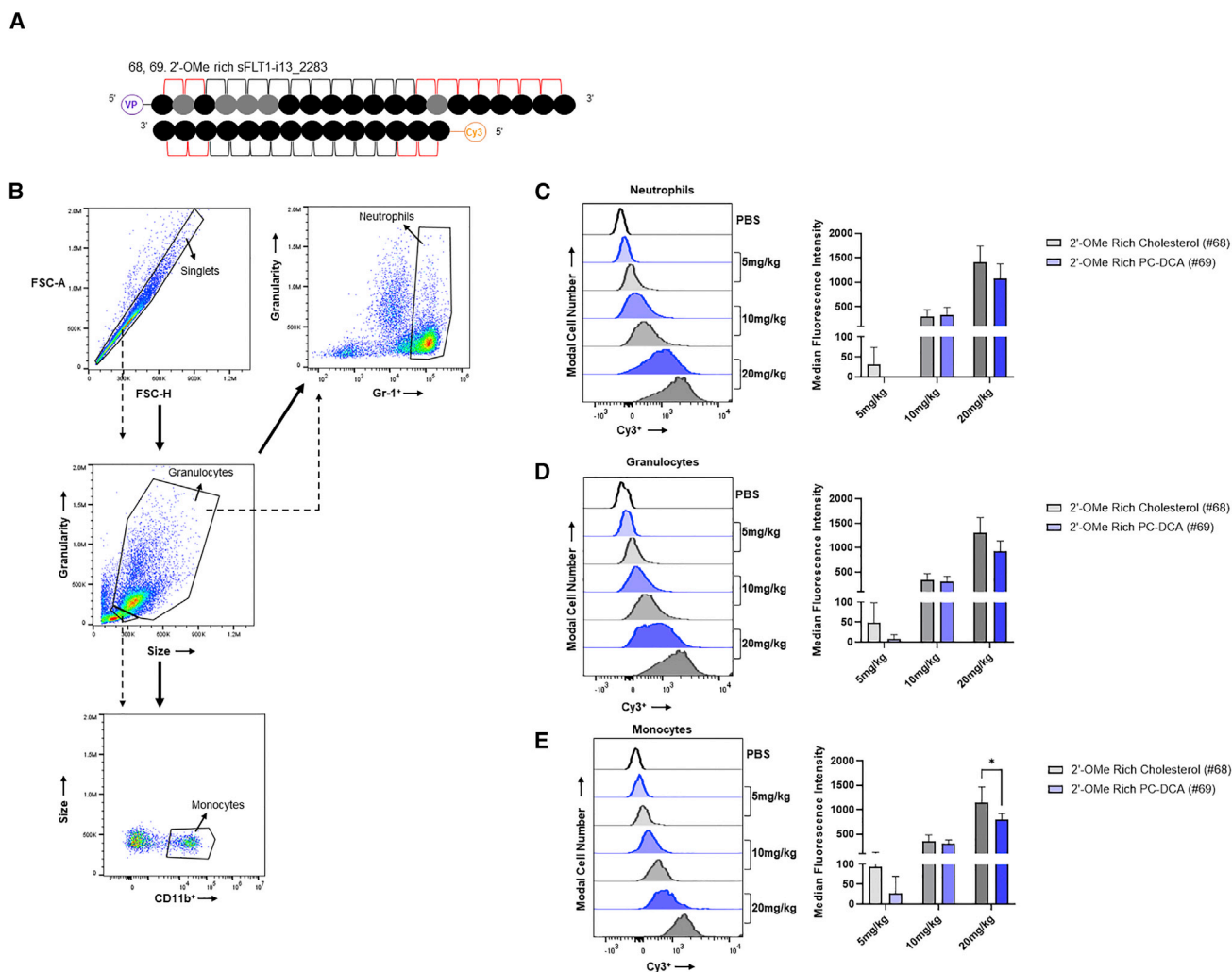


Figure 6. PC-DCA conjugated siRNA show lower accumulation in bone marrow immune cells

FACS analysis of bone marrow cells of CD1 mice injected with Cy3 labeled sFLT1-13_2283 siRNA variants. (A) Schematic of the siRNA chemical scaffold used in this experiment. (B) Gating scheme used to quantify Cy3 intensity of specific cell populations in the bone marrow in (B), (C), and (D). (C–E) Frequency distribution histogram of Cy3 fluorescence intensity (left) and bar graphs of Cy3 median fluorescence intensity (right) of bone marrow (C) neutrophils, (D) granulocytes, and (E) monocytes 24 h post-injection of siRNA variants ($n = 3$, means \pm SDs). p values describe statistically significant differences between compounds (1-way ANOVA; * $p < 0.05$; non-significant differences unmarked).

conjugated siRNA in each cell population were measured using FlowJo software.

For both PC-DCA and Chol siRNA, a dose-dependent shift in $Cy3^+$ population distribution was observed in neutrophils, granulocytes, and monocytes (Figures 6C–6E, histograms). The rightward shifts in population distribution, indicative of the number of cells transfected by the siRNA, was greater for Chol siRNA (gray histograms) compared to PC-DCA siRNA (blue histograms) for all injected doses in all three cell populations. In neutrophils, the median fluorescence intensity (MFI) of cells (Figure 6C, bar graphs) was higher for Chol siRNA compared to PC-DCA siRNA at 5 mg/kg (Chol: 30.8 MFI; PC-DCA: 0.3 MFI) and 20 mg/kg (Chol: 1,402.0 MFI; PC-DCA:

1,076.0 MFI) doses, consistent with the increase in the number of transfected cells by Chol siRNA (versus PC-DCA siRNA). The same was true in granulocytes (Figure 6D, bar graphs) at 5 mg/kg (Chol: 48.9 MFI; PC-DCA: 6.8 MFI) and 20 mg/kg (Chol: 1,300.0 MFI; PC-DCA: 916.3 MFI) doses. Interestingly, in both neutrophils and granulocytes, the median fluorescence intensity for Chol and PC-DCA siRNA groups were similar at the 10 mg/kg dose (neutrophils—Chol: 294.0 MFI; PC-DCA: 334.7 MFI; granulocytes—Chol: 328.3 MFI; PC-DCA: 306.3 MFI). In monocytes, which are the primary effectors of a cytokine response, the differences in the number of cells transfected (Figure 6E, histogram) and MFI (Figure 6E, bar graph) between the Chol and PC-DCA siRNA treated mice were clearer. At 5 and 20 mg/kg, the MFI of monocytes was higher in

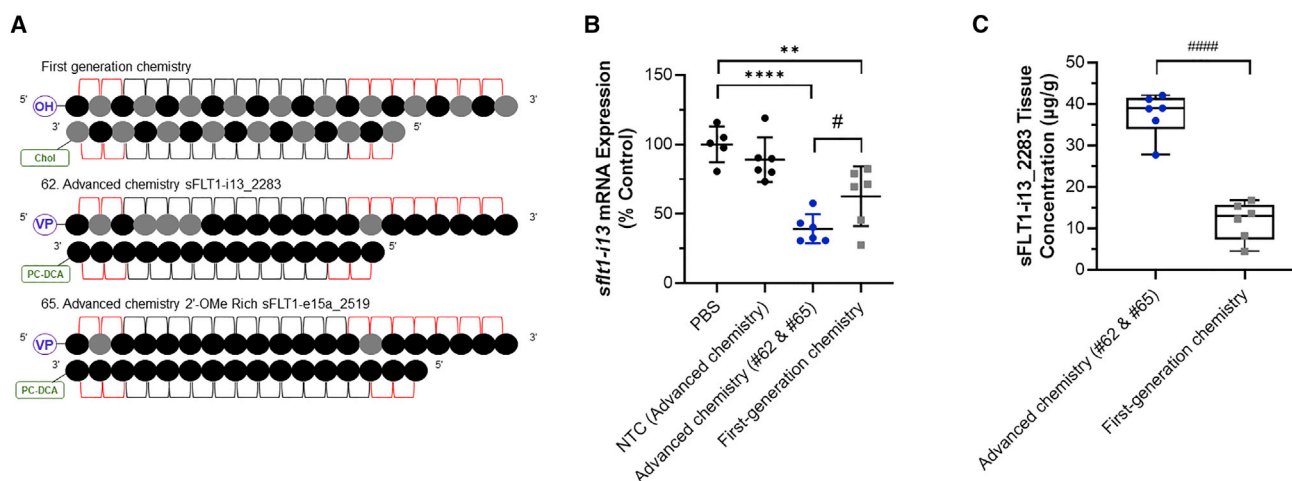


Figure 7. Optimization of 5'-moiety, 2'-ribose modification pattern and conjugate results in increased tissue accumulation and silencing efficiency *in vivo*

Pregnant CD1 mice injected with a mixture of 20 mg/kg sFLT1-i13_2283 and 20 mg/kg sFLT1-e15a_2519 siRNA variants on E13 and E14. (A) Schematic of the chemical pattern of siRNA compounds injected. (B) *sflt1-i13* mRNA levels in placenta on E18 measured using the Quantigene 2.0 RNA Assay. Levels were normalized to *Ft1* and presented as percentage of PBS control ($n = 6$, means \pm SDs). (C) Amount of sFLT1-i13_2283 siRNA accumulation in the placenta on E18 measured using PNA hybridization assay ($n = 6$). p values describe statistically significant differences between compounds (1-way ANOVA; ** $p < 0.01$; **** $p < 0.0001$; non-significant differences unmarked. Unpaired t test; # $p < 0.05$; #### $p < 0.0001$).

Chol siRNA treated mice, with the difference being statistically significant at 20 mg/kg (5 mg/kg—Chol: 93.3 MFI; PC-DCA: 26.4 MFI; 20 mg/kg—Chol: 1,147.0 MFI; PC-DCA: 793.3 MFI, $p < 0.04$). At 10 mg/kg, a smaller difference in MFI was observed (Chol: 353.7 MFI; PC-DCA: 299.7 MFI).

As PC-DCA supports better functional accumulation of siRNA in the placenta with reduced delivery to bone marrow immune cells, we selected PC-DCA as the optimal conjugate for further evaluation.

Systematic chemical optimization of *sFLT1*-targeting siRNAs improves placental accumulation and degree of *sFLT1* silencing with a better safety profile

With the development of our chemically advanced scaffolds (Figure 7A, siRNA 62 and 65), we performed a head-to-head comparison with the first-generation *sFLT1*-targeting siRNAs (Figure 7A; Table S1) in pregnant mice.²¹ Even though a 1:1 mixture of sFLT1-i13_2283 and sFLT1-e15a_2519 was tested, the silencing efficiency data shown in Figure 7 correspond to the activity of sFLT1-i13_2283 alone since that is the only target expressed in mice. After subcutaneous injection of 20 mg/kg of each compound into mice, we observed increased silencing of placental *sFLT1-i13* by the advanced siRNA compared to the first-generation siRNA (39% versus 63%, $p < 0.05$; Figure 7B) and a 3-fold increase in placental accumulation (37 $\mu\text{g/g}$ versus 12 $\mu\text{g/g}$, $p < 0.0001$; Figure 7C).

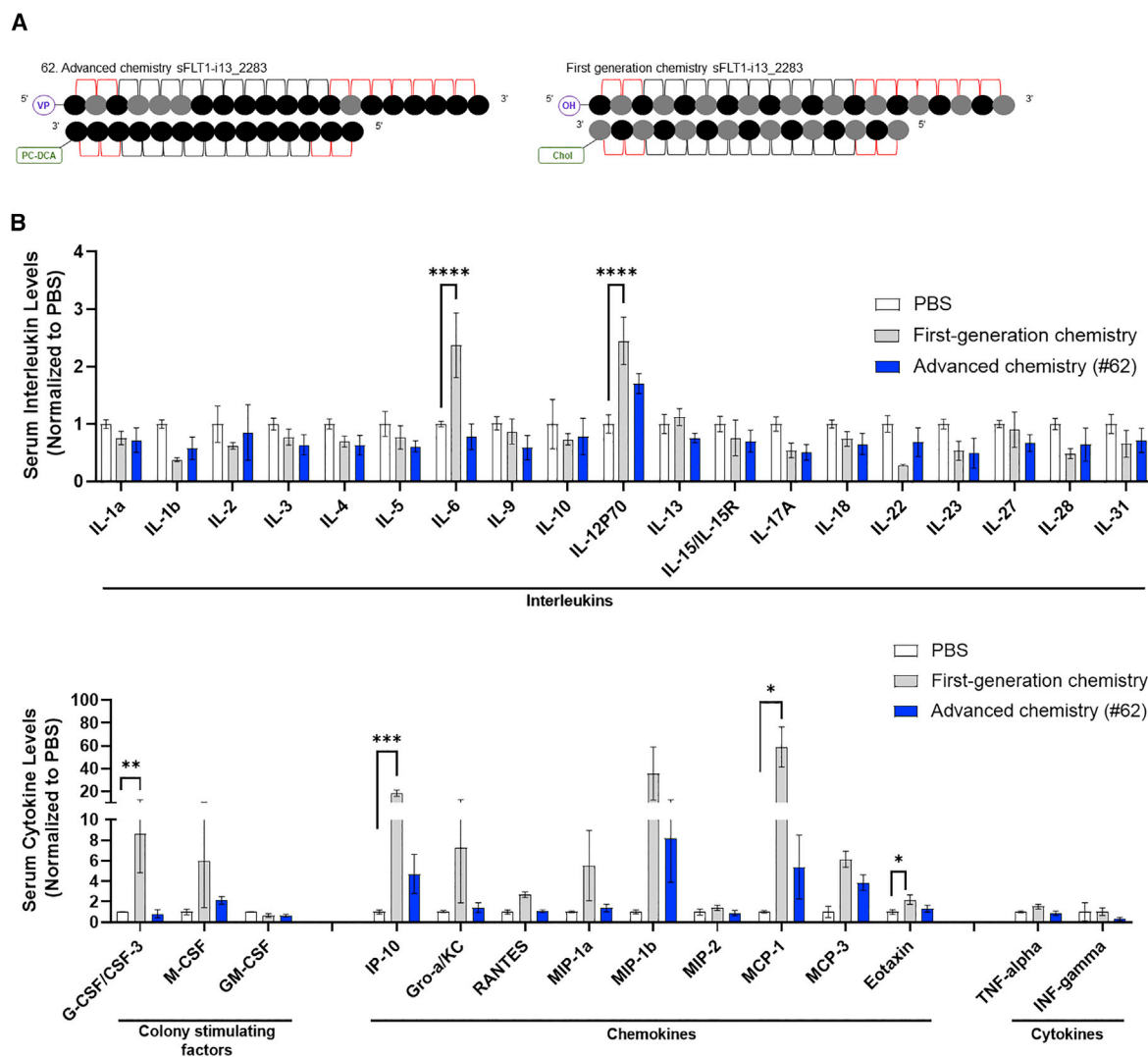
Because immune cell accumulation may be influenced by duplex asymmetry and 2'-OMe content, not just conjugate chemistry, we compared the acute serum cytokine response to a high dose (75 mg/kg) of the advanced chemistry siRNA (siRNA 62) versus the first-generation siRNA (Figure 8A; Table S1). While the levels

of most interleukins (ILs) did not change, a significant increase in serum IL-6 and IL-12 levels was observed in mice treated with the first-generation siRNA compared to phosphate buffered saline (PBS) control (IL-6: 2.4, $p < 0.0001$; IL-12: 2.4, $p < 0.0001$). The advanced siRNA did not stimulate IL-6 levels but caused a non-significant increase in IL-12 levels (IL-6: 0.8, IL-12: 1.7) (Figure 8B). These collective results are consistent with our observation of relatively higher accumulation of Chol siRNA in monocytes, but we were surprised to see that the advanced siRNA did not show any IL-6 stimulation, given that we did see some accumulation of PC-DCA siRNA in monocytes at higher doses (Figure 6E). Further research is necessary to elucidate the relationship between siRNA chemistry and interleukin stimulation pathways.

The first-generation compound also showed a significant increase in colony-stimulating factors (CSFs), such as granulocyte CSF/CSF-3 (8.7, $p < 0.01$), and in chemokines, such as interferon- γ -inducible protein 10 (IP-10) (18.4, $p < 0.001$), monocyte chemoattractant protein-1 (MCP-1) (58.9, $p < 0.05$) and eotaxin (2.2, $p < 0.05$). Although treatment with the advanced siRNA also caused increases in M-CSF (2.1), IP-10 (4.7), macrophage inflammatory protein (MIP)-1b (8.2), and MCP-1 (5.4) (not statistically significant), these levels were consistently lower compared to that of the first-generation siRNA group (Figure 8B).

DISCUSSION

There remains an unmet need for the development of a PE therapeutic. We previously demonstrated siRNA-mediated silencing of placental *sFLT1* mRNAs as a viable therapeutic approach. Here, we demonstrate that a combination of 5' moiety, 2'-OMe content, duplex asymmetry, and conjugate chemistry optimization can significantly



enhance placental delivery, silencing efficiency, and safety of RNAi-based modulation of *sFLT1*. Findings from this study further advance *sFLT1*-targeting siRNA therapies toward the clinic.

While the GalNac conjugate is the basis of currently approved siRNA drugs (i.e., givosiran),^{69,70} it delivers to the liver only.^{71–73} Several strategies are being explored to achieve extrahepatic delivery, including antibody conjugates,^{74,75} peptide conjugates,^{76,77} multivalency,³⁹ and hydrophobic conjugates.³⁰ DIO is widely distributed and retained in mouse brains compared to mono-siRNA, likely due to its increased size and cooperativity of PS-driven cellular uptake,³⁹ but multivalency did not support placental delivery (Figure 2). Instead, lipid conjugation is necessary to deliver siRNAs to placenta.

Using PC-DCA instead of a Chol conjugate enhanced siRNA delivery to the placenta while maintaining similar delivery to liver and kidney (Figures 2 and S1). In general, the more hydrophobic conjugates showed a trend for increased placental accumulation compared to the less hydrophobic conjugates, which is likely due to hydrophobicity-driven serum binding profiles.^{24,30} However, the accumulation of PC-DCA siRNA was significantly higher than DCA and Chol siRNA, despite being the least hydrophobic of the three.³⁰ This result suggests that a choline moiety on hydrophobic conjugates may further drive placental accumulation. The placental extracellular matrix is rich in heparan sulfate, a complex acidic glycosaminoglycan with negatively charged side chains.⁷⁸ It is possible that these side chains are involved in electrostatic interactions with the positive charge of the choline

moiety to increase accumulation in placenta. Further investigation is required to investigate the role of positive charge in placental entry.

Consistent with previous reports, the impact of duplex symmetry on *in vitro* activity is sequence dependent.^{31,41} Indeed, we found that using a 20-nt symmetric duplex instead of a 20-nt/15-nt asymmetric structure reduces target silencing for sFLT1-i13_2283, but not sFLT1-e15a_2519. sFLT1-i13_2283 may benefit from the lower thermodynamic stability offered by a shorter passenger strand because it has higher G/C content at the 3' end of the guide strand (5 of 7 residues are G/C) compared to sFLT1-e15a_2519 (2 of 7 residues are G/C), potentially reducing the efficiency of duplex unwinding. However, further investigation is required to understand the interplay between sequence and duplex asymmetry. We also confirm that the extent of duplex asymmetry should be limited, even for sequences that benefit from it.^{31,41} For both sFLT1-i13_2283 and sFLT1-e15a_2519, the use of 12-nt passenger strands entirely inhibits activity.

The majority of clinical-stage compounds possess a larger fraction of 2'-OMe modifications than 2'-F modifications.⁷⁹ 2'-OMe is more stabilizing against nucleases than 2'-F,⁴⁵ and increasing 2'-OMe content enhances siRNA potency and the duration of effect *in vivo* for some sequences.³³ Here, we observed that introducing 2'-OMe in the guide strand had a negative impact on activity. However, in some cases, pairing 2'-OMe-rich guide strands with 2'-OMe-rich passenger strands improved activity (Figure S3), suggesting that chemical modification patterns of the guide and passenger strands should be optimized in tandem. 2'-OMe rich scaffolds with very limited 2'-F (86% or 94% 2'-OMe per molecule) demonstrated *in vitro* activities comparable to that of the original 2'-OMe/2'-F scaffold (Figure 4) in a sequence-specific manner. sFLT1-e15a_2519 maintained full potency, but sFLT1-i13_2283 decreased slightly. As 2'-F incorporation is a point of safety concern,⁸⁰ reducing 2'-F content to less than 15% is exciting and may generate a stable, safe clinical candidate. Nevertheless, because 2'-OMe tolerance is sequence dependent, identifying additional 2'-OMe-rich siRNAs will require extensive screening.

Using the 5'-VP modification further enhanced silencing efficiency (Figure 5). However, the degree of improvement, both in accumulation and levels of silencing, was relatively small (extra 13 µg/g accumulation; 14% difference in mRNA expression). Thus, 5'-VP is likely not needed for delivery to tissues with high siRNA accumulation. Indeed, the FDA-approved, fully modified GalNAc siRNA givosiran⁶⁹ contains a 5'-OH modification⁷⁰ and induces long-term silencing in liver.⁷¹⁻⁷³ However, in tissues with lower siRNA accumulation, such as placenta, even small improvements could be clinically significant (Figures 2 and S1). Future work should explore the clinical significance of 5'-VP incorporation in tissues of low siRNA accumulation.

Combining 5'-VP, 2'-OMe-rich content, sequence-specific duplex asymmetry, and the PC-DCA conjugate into sFLT1-targeting

siRNAs significantly improved *in vivo* silencing efficiency in mouse placenta compared to the first-generation compound (Figure 7). We also observed that PC-DCA compound was better tolerated than the Chol siRNA, with pronounced activation of select interleukins, CSFs, and chemokines with the Chol compound (Figure 8). Despite the vast majority of injected Chol siRNA accumulating in liver, no changes in liver damage markers (e.g., amino-transferases) were observed.²¹ Thus, the dose-limited toxicity is likely related to the significant transduction of bone marrow monocytes. The shift to PC-DCA from Chol significantly decreases monocyte transduction (Figure 6), translating into better tolerability. Collectively, these findings are clinically significant; with the ability to deliver fully modified, conjugated siRNAs to a wide range of tissues (including immune cells), it is critical to find a conjugate that balances optimal activity with minimal toxicity.

The RNAi therapeutics field is exploding and hydrophobic conjugation of fully modified siRNAs is paving a way as a class of compounds with a promising therapeutic future.^{30,81} The optimization approach presented in this study provides a framework for modulating factors to test fully modified conjugated siRNAs and advance them toward the clinic.

MATERIALS AND METHODS

Oligonucleotide synthesis

Oligonucleotides were synthesized by phosphoramidite solid-phase synthesis using modified (2'-F, 2'-O-Me) phosphoramidites with standard protecting groups, on a MerMade12 (Biosearch Technologies, Novato, CA) or on a Dr Oligo 48 (Biolytic, Fremont, CA), using modified protocols. Phosphoramidites were prepared at 0.1 M in anhydrous acetonitrile (ACN), with added dry 15% dimethylformamide in the 2'-OMe-uridine amidite. 5-(Benzylthio)-1H-tetrazole (BTT) was used as the activator at 0.25 M. Detritylations were performed using 3% trichloroacetic acid in dichloromethane. The capping reagents used were CAP A, 20% n-methylimidazole in ACN, and CAP B, 20% acetic anhydride, 30% 2,6-lutidine in ACN (synthesis reagents were purchased at AIC, Westborough, MA). Sulfurization was performed with a 0.1-M solution of 3-[(dimethylaminomethylene)amino]-3H-1,2,4-dithiazole-5-thione (DDTT) in pyridine (Chemgenes, Wilmington, MA) for 4 min. Phosphoramidite coupling times were 4 min. 5'-Vinyl tetra phosphonate (pivaloyloxymethyl) 2'-O-methyl uridine 3'-CE phosphoramidite (VP) was used for the 5'-vinyl-phosphonate coupling when needed. Cy3 phosphoramidite (Quasar 570 CE) was purchased from GenePharma (Shanghai, China). All of the other amidites were purchased from Chemgenes. Unconjugated oligonucleotides were synthesized on 500-Å long-chain alkyl amine (LCAA) controlled pore glass (CPG) functionalized with Unylinker terminus (Chemgenes). Cholesterol-conjugated oligonucleotides were made on a 500-Å LCAA-CPG support, where the cholesterol moiety is bound to tetra-ethylenglycol through a succinate linker (Chemgenes). Divalent oligonucleotides (DIO) were synthesized on a modified solid support.³⁹ DCA-, DHA-, and PC-DCA-conjugated oligonucleotides were synthesized on a modified solid support.³⁰

Deprotection and purification of oligonucleotides for sequence screening

The columns containing unconjugated and cholesterol-conjugated oligonucleotides attached to the solid support were deprotected 1 h at room temperature with methylamine gas (Airgas). Columns with deprotected oligonucleotides were rinsed out with a mixture of 0.1 M sodium acetate in 85% ethanol, followed by 85% ethanol wash, the excess ethanol was dried from the columns, and the oligonucleotides were flushed out in water.

Deprotection and purification of oligonucleotides for *in vivo* experiments

Conjugated and Cy3-labeled oligonucleotides were cleaved and deprotected in 28%–30% ammonium hydroxide and 40% aqueous methylamine (AMA) in a 1:1 ratio for 2 h at room temperature. The VP-containing oligonucleotides were cleaved and deprotected as previously described.⁸² Briefly, CPG with VP oligonucleotides was treated with a solution of 3% diethylamine in 28%–30% ammonium hydroxide at 35°C for 20 h.

The solutions containing cleaved oligonucleotides were filtered to remove the CPG and dried under vacuum. The resulting pellets were re-suspended in 5% ACN in water. Purifications were performed on an Agilent 1290 Infinity II HPLC system. VP- and DIO-conjugated oligonucleotides were purified using a custom 20 × 150 mm column packed with Source 15Q anion exchange resin (Cytiva, Marlborough, MA); run conditions: eluent A, 10 mM sodium acetate in 20% ACN in water; eluent B, 1 M sodium perchlorate in 20% ACN in water; linear gradient, 10%–35% B for 30 min at 40°C. Hydrophobic-conjugated and Cy3-labeled oligonucleotides were purified using a 21.2 × 150-mm PRP-C18 column (Hamilton, Reno, NV); run conditions: eluent A, 50 mM sodium acetate in 5% ACN in water; eluent B, 100% ACN; linear gradient, 25%–60% B for 30 min at 60°C. Flow was 30 mL/min in both methods and peaks were monitored at 260 nm and for labeled oligos at 550 nm. Fractions were analyzed by liquid chromatography-mass spectrometry (LC-MS), and pure fractions were dried under vacuum. Oligonucleotides were re-suspended in 5% ACN and desalted by size exclusion on a 25 × 250-mm custom column packed with Sephadex G-25 media (Cytiva) and lyophilized.

LC-MS analysis of oligonucleotides

The identity of oligonucleotides was verified by LC-MS analysis on an Agilent 6530 accurate mass Q-TOF using the following conditions: buffer A: 100 mM 1,1,1,3,3,3-hexafluoroisopropanol (HFIP) and 9 mM triethylamine (TEA) in LC-MS grade water; buffer B: 100 mM HFIP and 9 mM TEA in LC-MS grade methanol; column, Agilent AdvanceBio oligonucleotides C18; linear gradient 0%–30% B 8 min (VP and DIO); 50%–100% B 8 min (hydrophobic conjugated and labeled oligos); temperature, 60°C; flow rate, 0.5 mL/min. LC peaks were monitored at 260 nm and for labeled oligos at 550 nm. MS parameters: Source, electrospray ionization; ion polarity, negative mode; range, 100–3,200 *m/z*; scan rate, 2 spectra/s; capillary voltage, 4,000; fragmentor, 180 V.

Deprotection, purification, and LC-MS reagents were purchased from Fisher Scientific, Sigma-Aldrich, and Oakwood Chemicals.

MS characterization of siRNA strands used for *in vivo* experiments are shown in [Figures S6–S8](#).

Injection of conjugated siRNAs into mice

Animal experiments were performed in accordance with animal care ethics approval and guidelines of the University of Massachusetts Medical School Institutional Animal Care and Use Committee (IACUC, protocol no. A-2411) and the Beth Israel Deaconess Medical Center IACUC Committee (protocol no. 027-2020). Female CD1 mice at 6–8 weeks of age (The Jackson Laboratory, Bar Harbor, ME) received an intrascapular subcutaneous injection with 150 μ L PBS (PBS controls) or with the indicated amount of siRNA (unconjugated or lipid conjugated) suspended in 150 μ L PBS. Pregnant females were injected on embryonic day (E)13 and/or E14.

Fluorescence microscopy

At 48 h post-injection, mice were euthanized (0.5 mL ketamine and xylazine mixture/mouse) and perfused with PBS. Tissues were collected and immersed in 10% formalin solution overnight at 4°C. Tissues were embedded in paraffin and sliced into 4- μ m sections that were mounted on glass slides. Tissue sections on glass slides were deparaffinized by incubating twice in xylene for 8 min. Sections were rehydrated in an ethanol series from 100% to 95%–80%, for 4 min each. Slides were then washed with PBS for 2 min, incubated with DAPI (250 ng/mL, Molecular Probes, Eugene, OR) in 10× PBS for 2 min, and washed again in PBS for 2 min. Slides were mounted with PermaFluor mounting medium (Molecular Probes) coverslips and dried overnight at 4°C. Sections were imaged at 10× using a Leica DM5500B microscope (Leica, Wetzlar, Germany) fitted with a DFC365 FX fluorescence camera.

PNA hybridization assay

Tissue concentrations of antisense strands were determined using a PNA hybridization assay.^{40,83} Tissues (liver, kidney 5 mg; placenta 13 mg) were placed in QIAGEN (Hilden, Germany) collection microtubes holding 3-mm tungsten beads and lysed in 200 μ L MasterPure tissue lysis solution (EpiCentre) containing 0.2 mg/mL proteinase K (Invitrogen, Carlsbad, CA) using a QIAGEN TissueLyser II. Lysates were then centrifuged at 1,000 × *g* for 10 min and incubated for 1 h at 55°C–60°C. Sodium dodecyl sulfate (SDS) was precipitated from lysates by adding 30 μ L 3 M potassium chloride and pelleted centrifugation at 5,000 × *g* for 15 min. Conjugated siRNAs in cleared supernatant were hybridized to a Cy3-labeled PNA probe fully complementary to the antisense strand (PNABio, Thousand Oaks, CA). Samples were analyzed by high-performance liquid chromatography (HPLC) (Agilent, Santa Clara, CA) over a DNAPac PA100 anion-exchange column (Thermo Fisher Scientific, Waltham, MA), in a gradient of sodium perchlorate, as follows: Buffer A: 50% water; 50% ACN; 25 mM Tris-HCl, pH 8.5; 1 mM ethylenediaminetetraacetate. Buffer B: 800 mM sodium perchlorate in buffer A. Gradient conditions: 10% buffer B within 4 min, 50% buffer B for 1 min, and

50%–100% buffer B within 5 min. Cy3 fluorescence was monitored and peaks integrated. Final concentrations were ascertained using calibration curves generated by spiking known quantities of lipid-conjugated siRNA into tissue lysates from an untreated animal. Representative PNA standard curves for siRNA quantitation in tissues are shown in [Figure S4](#). Spiked samples for calibration and experimental samples were processed and analyzed under the same laboratory conditions. Representative HPLC chromatograms used for PNA quantification of siRNA in tissues are shown in [Figure S5](#).

Cell culture (HeLa and WM-115 cells)

HeLa cells (ATCC, #CCL-2) were maintained in Dulbecco's modified Eagle's medium (DMEM) (Cellgro, #10-013CV) and WM-115 cells (ATCC CRL-1676) were maintained in Eagle's minimum essential medium (EMEM) (Sigma-Aldrich, M0643). The media was supplemented with 9% fetal bovine serum (FBS) (#26140, Gibco, Waltham, MA), and all of the cells were grown at 37°C and 5% CO₂. Cells were split every 2–7 days, and discarded after 15 passages.

Transfection of sFLT1-i13 and sFLT1-e15a target sequences into HeLa cells

cDNA sequences corresponding to 20-nt-long, unique regions of sFLT1-i13 and/or sFLT1-e15a target mRNAs (see [Table S2](#)) were cloned into psiCheck-2 vectors (C8021, Promega, Madison, WI) according to the manufacturer's protocol. HeLa cells were plated (3⁶ or 6⁶ cells/10-cm dish; see [Table S2](#)) and grown overnight (O/N) to ~80% confluency before being transfected with 24 µg psiCheck-2 plasmid. Transfections were performed using Lipofectamine 2000 (11668019, Invitrogen) according to the manufacturer's protocol. Transfected cells were grown O/N before transfer and treatment with siRNAs.

Direct delivery (i.e., passive uptake) of oligonucleotides

Transfected HeLa cells were diluted to 8,000–10,000 cells/50 µL DMEM containing 6% FBS; WM-115 cells were diluted to 25,000 cells/50 µL EMEM containing 4.5% FBS. siRNAs were diluted to twice the maximum test concentration in OptiMEM (31985-088, Carlsbad, CA;) and serially diluted to create 7-point dose responses (see [Table S2](#) for dilution scheme). Diluted siRNA 50 µL was added to 50 µL diluted cells in 96-well cell culture-treated plates, resulting in a final concentration of 1.5 µM siRNA for the maximum dose and 3% or 2.25% FBS. Cells were incubated for 72 h at 37°C and 5% CO₂.

Method for quantitative analysis of target mRNA expression

HeLa cells: mRNA was quantified using the Dual-Glo Luciferase Assay System according to the manufacturer's protocol (#E2940, Promega). Luminescence was detected on a Veritas Luminometer (#998-9100, Promega) or a Tecan M1000 (Tecan, Morrisville, NC). For each cell treatment plate, control reporter (fLuc) was used as a normalization control, and data were plotted as a percentage of the mean results from untreated cells.

WM-115 cells: mRNA was quantified using the QuantiGene 2.0 assay kit (QS0011, Affymetrix, Santa Clara, CA). Cells were lysed in 250 µL diluted lysis mixture composed of 1 part lysis mixture (13228, Affy-

metrix), 2 parts H₂O, and 0.167 µg/µL proteinase K (QS0103, Affymetrix), for 30 min at 55°C. Probe sets for human *sFLT1-i13*, *sFLT1-e15a*, and *HPRT* (SA-50459, SA-50496, SA-10030, Affymetrix) were diluted and used according to the manufacturer's recommended protocol. Cell lysates were mixed thoroughly before 20–60 µL lysate and 20 µL probe set mixture were added to each well of a capture plate in triplicate. Lysis mixture, 20–60 µL, diluted in 2 parts H₂O was also added, such that each well contained 100 µL total. For each cell treatment plate, *HPRT* was used as a normalization control, and data were plotted as a percentage of the mean results from untreated cells.

Immune cell isolation and FACS analysis

Eight-week-old female mice were injected subcutaneously with a panel of Cy3-labeled siRNA variants. After 24 h, mouse femur bone was dissected and femur bone marrow cells were isolated by flushing dissected femur bones with PBS using a 23-G needle onto a 40-µm cell strainer placed in a 50-mL conical tube. The bone marrow was then smashed using a 5-mL plunger, followed by rinsing of the strainer with PBS. The cell solution collected in the 50-mL tube was centrifuged at 350 g for 5 min at room temperature and washed once with PBS. Cell numbers were adjusted to 10⁷ cells/mL, and 100 µL of these cells were stained with FITC-CD11b (#11-0118-42, eBioscience, Hatfield, UK) and Pacific Blue-GR-1 (#RM3028, Invitrogen) antibodies according to the manufacturer's recommendations to identify cell populations. Cells were analyzed using Cytoflex LX (Beckman Coulter Life Sciences, Indianapolis, IN) and gated appropriately to identify singlets, CD11b⁺ monocytes, and Gr-1⁺ granulocytes. The compensation matrix was defined based on single-color controls. All graphical and statistical analyses were performed using FlowJo according to the manufacturer's instructions.

Serum cytokine measurements

Blood was collected from mice 24 h post-injection via cardiac puncture in a serum separator tube, allowed to stand at room temperature for 10 min and then centrifuged at 1,500 × g for 10 min at 4°C to separate the serum from other blood components. The serum was then analyzed for cytokine levels using the Cytokine & Chemokine 36-Plex Mouse ProcartaPlex Panel 1A (Invitrogen) according to the manufacturer's instructions.

Statistical analyses

Dose-response data were analyzed using GraphPad Prism 9.0 software (GraphPad Software, San Diego, CA). Concentration-dependent IC₅₀ curves fitted using the log(inhibitor) versus response – variable slope (4 parameters) method. The lower limit of the curve was set to >0, and the upper limit of the curve was set to a constant = 100. AUCs calculated using automatic software settings (i.e., baseline: Y = 0, minimum peak height: ignore peaks <10% of the distance from Y_{min} to Y_{max}). Statistical outliers were identified using Q = 1% and were excluded from the calculations of the fitted curve and AUC.

SUPPLEMENTAL INFORMATION

Supplemental information can be found online at <https://doi.org/10.1016/j.omtn.2022.06.009>.

ACKNOWLEDGMENTS

The work was supported by grants R35 GM131839, R01 HD086111, and S10 OD 020012. All of the work was completed at the University of Massachusetts Medical School, Worcester, MA and at the Beth Israel Deaconess Medical Center, Boston, MA.

AUTHOR CONTRIBUTIONS

S.M.D. conducted the PNA experiments in Figure 2, designed and conducted *in vitro* concentration-response experiments, and drafted the manuscript. V.N.H. designed and conducted the *in vivo* experiments for sFLT1-targeting siRNAs and helped write and edit the manuscript. A.L. conducted *in vivo* experiments for sFLT1-targeting siRNAs, FACS analysis, and the multiplex cytokine/chemokine assay, and edited the manuscript. D.E., J.S., and N.M. synthesized oligonucleotides for HTT_10,150, sFLT1-i13_2283, and sFLT1-e15a_2519 siRNAs. A.B. synthesized the CPG for lipid-conjugated siRNAs. A.A.T. and J.F.A. conceived the 2'-OMe-rich chemical modification patterns used for the 20-/15-mer sFLT1-i3_2283 and sFLT1-e15a_2519 siRNAs (Figure 4); A.A.T. also completed the microscopy experiments shown in Figures 2 and S1. S.A.K., M.J.M., and A.K. guided the study designs, and A.K. also helped to draft the manuscript. Dr. Emily Haberlin reviewed the manuscript.

DECLARATION OF INTERESTS

A.K. and J.F.A. are inventors on *Fully Stabilized Asymmetric siRNA*, US Utility Application No. 15/089,423; A.K., A.A.T., M.J.M., and S.A.K. are inventors on *Oligonucleotide compounds for treatment of preeclampsia and other angiogenic disorders*, US Utility Application No. 16/675,369; A.K., S.M.D., A.A.T., and J.F.A. are inventors on *O-Methyl Rich Fully Stabilized Oligonucleotides*, US Utility Application No. 16/550,076; A.K., S.M.D., V.N.H., and S.A.K. are inventors on *Optimized Anti-FLT1 Oligonucleotide Compounds for Treatment of Preeclampsia and Other Angiogenic Disorders*, US Utility Application No. 63/214,224.

REFERENCES

- Sones, J.L., and Davisson, R.L. (2016). Preeclampsia, of mice and women. *Physiol. Genomics* 48, 565–572. <https://doi.org/10.1152/physiolgenomics.00125.2015>.
- Backes, C.H., Markham, K., Moorehead, P., Cordero, L., Nankervis, C.A., and Giannone, P.J. (2011). Maternal preeclampsia and neonatal outcomes. *J. Pregnancy* 2011, 214365. <https://doi.org/10.1155/2011/214365>.
- Wang, Y., Hao, M., Sampson, S., and Xia, J. (2017). Elective delivery versus expectant management for pre-eclampsia: a meta-analysis of RCTs. *Arch. Gynecol. Obstet.* 295, 607–622. <https://doi.org/10.1007/s00404-016-4281-9>.
- Mol, B.W.J., Roberts, C.T., Thangaratnam, S., Magee, L.A., de Groot, C.J.M., and Hofmeyr, G.J. (2016). Pre-eclampsia. *Lancet* 387, 999–1011. [https://doi.org/10.1016/S0140-6736\(15\)00070-7](https://doi.org/10.1016/S0140-6736(15)00070-7).
- Palmer, K.R., Tong, S., and Kaitu'u-Lino, T.J. (2017). Placental-specific sFLT-1: role in pre-eclamptic pathophysiology and its translational possibilities for clinical prediction and diagnosis. *Mol. Hum. Reprod.* 23, 69–78. <https://doi.org/10.1093/molehr/gaw077>.
- Maynard, S.E., Min, J.Y., Merchan, J., Lim, K.H., Li, J., Mondal, S., Libermann, T.A., Morgan, J.P., Sellke, F.W., Stillman, I.E., et al. (2003). Excess placental soluble fms-like tyrosine kinase 1 (sFlt1) may contribute to endothelial dysfunction, hypertension, and proteinuria in preeclampsia. *J. Clin. Invest.* 111, 649–658. <https://doi.org/10.1172/JCI17189>.
- Palmer, K.R., Kaitu'u-Lino, T.J., Hastie, R., Hannan, N.J., Ye, L., Binder, N., Cannon, P., Tuohy, L., Johns, T.G., Shub, A., and Tong, S. (2015). Placental-specific sFLT-1 e15a protein is increased in preeclampsia, antagonizes vascular endothelial growth factor signaling, and has antiangiogenic activity. *Hypertension* 66, 1251–1259. <https://doi.org/10.1161/HYPERTENSIONAHA.115.05883>.
- Fan, X., Rai, A., Kambham, N., Sung, J.F., Singh, N., Pettitt, M., Dhal, S., Agrawal, R., Sutton, R.E., Druzin, M.L., et al. (2014). Endometrial VEGF induces placental sFLT1 and leads to pregnancy complications. *J. Clin. Invest.* 124, 4941–4952. <https://doi.org/10.1172/JCI76864>.
- Vogtmann, R., Heupel, J., Herse, F., Matin, M., Hagmann, H., Bendix, I., Kraker, K., Dechend, R., Winterhager, E., Kimmig, R., et al. (2021). Circulating maternal sFLT1 (soluble fms-like tyrosine kinase-1) is sufficient to impair spiral arterial remodeling in a preeclampsia mouse model. *Hypertension* 78, 1067–1079. <https://doi.org/10.1161/HYPERTENSIONAHA.121.17567>.
- Chaiworapongsa, T., Romero, R., Espinoza, J., Bujold, E., Mee Kim, Y., Goncalves, L.F., Gomez, R., and Edwin, S. (2004). Evidence supporting a role for blockade of the vascular endothelial growth factor system in the pathophysiology of preeclampsia. Young Investigator Award. *Am. J. Obstet. Gynecol.* 190, 1541–1547. <https://doi.org/10.1016/j.ajog.2004.03.043>.
- Rana, S., Powe, C.E., Salahuddin, S., Verloren, S., Perschel, F.H., Levine, R.J., Lim, K.H., Wenger, J.B., Thadhani, R., and Karumanchi, S.A. (2012). Angiogenic factors and the risk of adverse outcomes in women with suspected preeclampsia. *Circulation* 125, 911–919. <https://doi.org/10.1161/CIRCULATIONAHA.111.054361>.
- Olsson, A.K., Dimberg, A., Kreuger, J., and Claesson-Welsh, L. (2006). VEGF receptor signalling - in control of vascular function. *Nat. Rev. Mol. Cell Biol.* 7, 359–371. <https://doi.org/10.1038/nrm1911>.
- Rana, S., Burke, S.D., and Karumanchi, S.A. (2020). Imbalances in circulating angiogenic factors in the pathophysiology of preeclampsia and related disorders. *Am. J. Obstet. Gynecol.* <https://doi.org/10.1016/j.ajog.2020.10.022>.
- Thadhani, R., Hagmann, H., Schaarschmidt, W., Roth, B., Cingoz, T., Karumanchi, S.A., Wenger, J., Lucchesi, K.J., Tamez, H., Lindner, T., et al. (2016). Removal of soluble fms-like tyrosine kinase-1 by dextran sulfate apheresis in preeclampsia. *J. Am. Soc. Nephrol.* 27, 903–913. <https://doi.org/10.1681/ASN.2015020157>.
- Thadhani, R., Kisner, T., Hagmann, H., Bossung, V., Noack, S., Schaarschmidt, W., Jank, A., Kribs, A., Cornely, O.A., Kreyssig, C., et al. (2011). Pilot study of extracorporeal removal of soluble fms-like tyrosine kinase 1 in preeclampsia. *Circulation* 124, 940–950. <https://doi.org/10.1161/CIRCULATIONAHA.111.034793>.
- Li, Z., Zhang, Y., Ying Ma, J., Kapoun, A.M., Shao, Q., Kerr, I., Lam, A., O'Young, G., Sannajust, F., Stathis, P., et al. (2007). Recombinant vascular endothelial growth factor 121 attenuates hypertension and improves kidney damage in a rat model of preeclampsia. *Hypertension* 50, 686–692. <https://doi.org/10.1161/HYPERTENSIONAHA.107.092098>.
- Makris, A., Yeung, K.R., Lim, S.M., Sunderland, N., Heffernan, S., Thompson, J.F., Iliopoulos, J., Killingsworth, M.C., Yong, J., Xu, B., et al. (2016). Placental growth factor reduces blood pressure in a uteroplacental ischemia model of preeclampsia in nonhuman primates. *Hypertension* 67, 1263–1272. <https://doi.org/10.1161/HYPERTENSIONAHA.116.07286>.
- Bergmann, A., Ahmad, S., Cudmore, M., Gruber, A.D., Wittschen, P., Lindenmaier, W., Christofori, G., Gross, V., Gonzalves, A., Grone, H.J., et al. (2010). Reduction of circulating soluble Flt-1 alleviates preeclampsia-like symptoms in a mouse model. *J. Cell Mol. Med.* 14, 1857–1867. <https://doi.org/10.1111/j.1582-4934.2009.00820.x>.
- Fire, A., Xu, S., Montgomery, M.K., Kostas, S.A., Driver, S.E., and Mello, C.C. (1998). Potent and specific genetic interference by double-stranded RNA in *Caenorhabditis elegans*. *Nature* 391, 806–811.
- Ashar-Patel, A., Kaymaz, Y., Rajakumar, A., Bailey, J.A., Karumanchi, S.A., and Moore, M.J. (2017). FLT1 and transcriptome-wide polyadenylation site (PAS) analysis in preeclampsia. *Sci. Rep.* 7, 12139. <https://doi.org/10.1038/s41598-017-11639-6>.
- Turanov, A.A., Lo, A., Hassler, M.R., Makris, A., Ashar-Patel, A., Alterman, J.F., Coles, A.H., Haraszi, R.A., Roux, L., Godinho, B., et al. (2018). RNAi modulation of placental sFLT1 for the treatment of preeclampsia. *Nat. Biotechnol.* <https://doi.org/10.1038/nbt.4297>.
- Allerson, C.R., Sioufi, N., Jarres, R., Prakash, T.P., Naik, N., Berdeja, A., Wanders, L., Griffey, R.H., Swayze, E.E., and Bhat, B. (2005). Fully 2'-modified oligonucleotide

- duplexes with improved in vitro potency and stability compared to unmodified small interfering RNA. *J. Med. Chem.* 48, 901–904. <https://doi.org/10.1021/jm049167j>.
23. Ly, S., Navaroli, D.M., Didiot, M.C., Cardia, J., Pandarinathan, L., Alterman, J.F., Fogarty, K., Standley, C., Lifshitz, L.M., Bellve, K.D., et al. (2017). Visualization of self-delivering hydrophobically modified siRNA cellular internalization. *Nucleic Acids Res.* 45, 15–25. <https://doi.org/10.1093/nar/gkw1005>.
 24. Osborn, M.F., Coles, A.H., Biscans, A., Haraszti, R.A., Roux, L., Davis, S., Ly, S., Echeverria, D., Hassler, M.R., Godinho, B., et al. (2019). Hydrophobicity drives the systemic distribution of lipid-conjugated siRNAs via lipid transport pathways. *Nucleic Acids Res.* 47, 1070–1081. <https://doi.org/10.1093/nar/gky1232>.
 25. Soutschek, J., Akinc, A., Bramlage, B., Charisse, K., Constien, R., Donoghue, M., Elbashir, S., Geick, A., Hadwiger, P., Harborth, J., et al. (2004). Therapeutic silencing of an endogenous gene by systemic administration of modified siRNAs. *Nature* 432, 173–178. <https://doi.org/10.1038/nature03121>.
 26. Byrne, M., Tzekov, R., Wang, Y., Rodgers, A., Cardia, J., Ford, G., Holton, K., Pandarinathan, L., Lapiere, J., Stanney, W., et al. (2013). Novel hydrophobically modified asymmetric RNAi compounds (sd-rxRNA) demonstrate robust efficacy in the eye. *J. Ocul. Pharmacol. Ther.* 29, 855–864. <https://doi.org/10.1089/jop.2013.0148>.
 27. Khan, T., Weber, H., DiMuzio, J., Matter, A., Dogdas, B., Shah, T., Thankappan, A., Disa, J., Jadhav, V., Lubbers, L., et al. (2016). Silencing myostatin using cholesterol-conjugated siRNAs induces muscle growth. *Mol. Ther. Nucleic Acids* 5, e342. <https://doi.org/10.1038/mtna.2016.55>.
 28. Alterman, J.F., Hall, L.M., Coles, A.H., Hassler, M.R., Didiot, M.C., Chase, K., Abraham, J., Sottosanti, E., Johnson, E., Sapp, E., et al. (2015). Hydrophobically modified siRNAs silence Huntingtin mRNA in primary neurons and mouse brain. *Mol. Ther. Nucleic Acids* 4, e266. <https://doi.org/10.1038/mtna.2015.38>.
 29. Nikan, M., Osborn, M.F., Coles, A.H., Godinho, B.M., Hall, L.M., Haraszti, R.A., Hassler, M.R., Echeverria, D., Aronin, N., and Khvorova, A. (2016). Docosahexaenoic acid conjugation enhances distribution and safety of siRNA upon local administration in mouse brain. *Mol. Ther. Nucleic Acids* 5, e344. <https://doi.org/10.1038/mtna.2016.50>.
 30. Biscans, A., Coles, A., Haraszti, R., Echeverria, D., Hassler, M., Osborn, M., and Khvorova, A. (2019). Diverse lipid conjugates for functional extra-hepatic siRNA delivery in vivo. *Nucleic Acids Res.* 47, 1082–1096. <https://doi.org/10.1093/nar/gky1239>.
 31. Hassler, M.R., Turanov, A.A., Alterman, J.F., Haraszti, R.A., Coles, A.H., Osborn, M.F., Echeverria, D., Nikan, M., Salomon, W.E., Roux, L., et al. (2018). Comparison of partially and fully chemically-modified siRNA in conjugate-mediated delivery in vivo. *Nucleic Acids Res.* 46, 2185–2196. <https://doi.org/10.1093/nar/gky037>.
 32. Biscans, A., Caiuzzi, J., Davis, S., McHugh, N., Sousa, J., and Khvorova, A. (2020). The chemical structure and phosphorothioate content of hydrophobically modified siRNAs impact extrahepatic distribution and efficacy. *Nucleic Acids Res.* 48, 7665–7680. <https://doi.org/10.1093/nar/gkaa595>.
 33. Foster, D.J., Brown, C.R., Shaikh, S., Trapp, C., Schlegel, M.K., Qian, K., Sehgal, A., Rajeev, K.G., Jadhav, V., Manoharan, M., et al. (2018). Advanced siRNA designs further improve in vivo performance of GalNAc-siRNA conjugates. *Mol. Ther.* 26, 708–717. <https://doi.org/10.1016/j.ymthe.2017.12.021>.
 34. Nair, J.K., Attarwala, H., Sehgal, A., Wang, Q., Aluri, K., Zhang, X., Gao, M., Liu, J., Indrakanti, R., Schofield, S., et al. (2017). Impact of enhanced metabolic stability on pharmacokinetics and pharmacodynamics of GalNAc-siRNA conjugates. *Nucleic Acids Res.* 45, 10969–10977. <https://doi.org/10.1093/nar/gkx818>.
 35. Balwani, M., Sardh, E., Ventura, P., Peiro, P.A., Rees, D.C., Stolz, U., Bissell, D.M., Bonkovsky, H.L., Windyga, J., Anderson, K.E., et al. (2020). Phase 3 trial of RNAi therapeutic givosiran for acute intermittent porphyria. *N. Engl. J. Med.* 382, 2289–2301. <https://doi.org/10.1056/NEJMoa1913147>.
 36. Prakash, T.P., Lima, W.F., Murray, H.M., Li, W., Kinberger, G.A., Chappell, A.E., Gaus, H., Seth, P.P., Bhat, B., Crooke, S.T., and Swayze, E.E. (2017). Identification of metabolically stable 5-phosphate analogs that support single-stranded siRNA activity. *Nucleic Acids Res.* 45, 6994. <https://doi.org/10.1093/nar/gkx381>.
 37. Parmar, R., Willoughby, J.L., Liu, J., Foster, D.J., Brigham, B., Theile, C.S., Charisse, K., Akinc, A., Guidry, E., Pei, Y., et al. (2016). 5'-(E)-Vinylphosphonate: a stable phosphate mimic can improve the RNAi activity of siRNA-GalNAc conjugates. *Chembiochem* 17, 985–989. <https://doi.org/10.1002/cbic.201600130>.
 38. Haraszti, R.A., Roux, L., Coles, A.H., Turanov, A.A., Alterman, J.F., Echeverria, D., Godinho, B., Aronin, N., and Khvorova, A. (2017). 5-Vinylphosphonate improves tissue accumulation and efficacy of conjugated siRNAs in vivo. *Nucleic Acids Res.* 45, 7581–7592. <https://doi.org/10.1093/nar/gkx507>.
 39. Alterman, J.F., Godinho, B., Hassler, M.R., Ferguson, C.M., Echeverria, D., Sapp, E., Haraszti, R.A., Coles, A.H., Conroy, F., Miller, R., et al. (2019). A divalent siRNA chemical scaffold for potent and sustained modulation of gene expression throughout the central nervous system. *Nat. Biotechnol.* 37, 884–894. <https://doi.org/10.1038/s41587-019-0205-0>.
 40. Roehl, I.S.M., and Seiffert, S. (2011). InventorOligonucleotide Detection Method Using a Peptide Nucleic Acid Probe.
 41. Chang, C.I., Yoo, J.W., Hong, S.W., Lee, S.E., Kang, H.S., Sun, X., Rogoff, H.A., Ban, C., Kim, S., Li, C.J., and Lee, D.K. (2009). Asymmetric shorter-duplex siRNA structures trigger efficient gene silencing with reduced nonspecific effects. *Mol. Ther.* 17, 725–732. <https://doi.org/10.1038/mt.2008.298>.
 42. Matranga, C., Tomari, Y., Shin, C., Bartel, D.P., and Zamore, P.D. (2005). Passenger-strand cleavage facilitates assembly of siRNA into Ago2-containing RNAi enzyme complexes. *Cell* 123, 607–620. <https://doi.org/10.1016/j.cell.2005.08.044>.
 43. Manoharan, M., Akinc, A., Pandey, R.K., Qin, J., Hadwiger, P., John, M., Mills, K., Charisse, K., Maier, M.A., Nechev, L., et al. (2011). Unique gene-silencing and structural properties of 2'-fluoro-modified siRNAs. *Angew Chem. Int. Ed. Engl.* 50, 2284–2288. <https://doi.org/10.1002/anie.201006519>.
 44. Wu, H., Ma, H., Ye, C., Ramirez, D., Chen, S., Montoya, J., Shankar, P., Wang, X.A., and Manjunath, N. (2011). Improved siRNA/shRNA functionality by mismatched duplex. *PLoS One* 6, e28580. <https://doi.org/10.1371/journal.pone.0028580>.
 45. Cummins, L.L., Owens, S.R., Risen, L.M., Lesnik, E.A., Freier, S.M., McGee, D., Guinasso, C.J., and Cook, P.D. (1995). Characterization of fully 2'-modified oligoribonucleotide hetero- and homoduplex hybridization and nuclease sensitivity. *Nucleic Acids Res.* 23, 2019–2024.
 46. Homsy, D., Monopoli, K.R., Betancur-Boissel, M., Shmushkovich, T., Wolfson, A.D., Leyfer, D., and Khvorova, A. (2018). Functional features defining the efficacy of cholesterol-conjugated, self-deliverable, chemically modified siRNAs. *Nucleic Acids Res.* 46, 10905–10916. <https://doi.org/10.1093/nar/gky745>.
 47. Chiu, Y.L. (2003). siRNA function in RNAi: a chemical modification analysis. *RNA* 9, 1034–1048. <https://doi.org/10.1261/rna.5103703>.
 48. Davis, S.M., Sousa, J., Vangieli, L., Hassler, M.R., Echeverria, D., Knox, E., Turanov, A.A., Alterman, J.F., and Khvorova, A. (2020). 2'-O-Methyl at 20-mer guide strand 3' termini may negatively affect target silencing activity of fully chemically modified siRNA. *Mol. Ther. Nucleic Acids* 21, 266–277. <https://doi.org/10.1016/j.omtn.2020.05.010>.
 49. Pozdeyev, N., Yoo, M., Mackie, R., Schweppe, R.E., Tan, A.C., and Haugen, B.R. (2016). Integrating heterogeneous drug sensitivity data from cancer pharmacogenomic studies. *Oncotarget* 7, 51619–51625. <https://doi.org/10.18632/oncotarget.10010>.
 50. Cummins, L.L., Owens, S.R., Risen, L.M., Lesnik, E.A., Freier, S.M., McGee, D., Guinasso, C.J., and Cook, P.D. (1995). Characterization of fully 2'-modified oligoribonucleotide hetero- and homoduplex hybridization and nuclease sensitivity. *Nucleic Acids Res.* 23, 2019–2024. <https://doi.org/10.1093/nar/23.11.2019>.
 51. Takahashi, M., Minakawa, N., and Matsuda, A. (2009). Synthesis and characterization of 2'-modified-4'-thioRNA: a comprehensive comparison of nuclease stability. *Nucleic Acids Res.* 37, 1353–1362. <https://doi.org/10.1093/nar/gkn1088>.
 52. Ma, J.B., Yuan, Y.R., Meister, G., Pei, Y., Tuschl, T., and Patel, D.J. (2005). Structural basis for 5'-end-specific recognition of guide RNA by the A. fulgidus Piwi protein. *Nature* 434, 666–670. <https://doi.org/10.1038/nature03514>.
 53. Frank, F., Sonenberg, N., and Nagar, B. (2010). Structural basis for 5'-nucleotide base-specific recognition of guide RNA by human AGO2. *Nature* 465, 818–822. <https://doi.org/10.1038/nature09039>.
 54. Boland, A., Tritschler, F., Heimstadt, S., Izaurralde, E., and Weichenrieder, O. (2010). Crystal structure and ligand binding of the MID domain of a eukaryotic Argonaute protein. *EMBO Rep.* 11, 522–527. <https://doi.org/10.1038/embor.2010.81>.

55. Lima, W.F., Prakash, T.P., Murray, H.M., Kinberger, G.A., Li, W., Chappell, A.E., Li, C.S., Murray, S.F., Gaus, H., Seth, P.P., et al. (2012). Single-stranded siRNAs activate RNAi in animals. *Cell* 150, 883–894. <https://doi.org/10.1016/j.cell.2012.08.014>.
56. Prakash, T.P., Lima, W.F., Murray, H.M., Elbashir, S., Cantley, W., Foster, D., Jayaraman, M., Chappell, A.E., Manoharan, M., Swayze, E.E., and Crooke, S.T. (2013). Lipid nanoparticles improve activity of single-stranded siRNA and gapmer antisense oligonucleotides in animals. *ACS Chem. Biol.* 8, 1402–1406. <https://doi.org/10.1021/cb4001316>.
57. Elkayam, E., Parmar, R., Brown, C.R., Willoughby, J.L., Theile, C.S., Manoharan, M., and Joshua-Tor, L. (2017). siRNA carrying an (E)-vinylphosphonate moiety at the 5' end of the guide strand augments gene silencing by enhanced binding to human Argonaute-2. *Nucleic Acids Res.* 45, 3528–3536. <https://doi.org/10.1093/nar/gkw1171>.
58. Sioud, M. (2006). Innate sensing of self and non-self RNAs by Toll-like receptors. *Trends Mol. Med.* 12, 167–176. <https://doi.org/10.1016/j.molmed.2006.02.004>.
59. Meng, Z., and Lu, M. (2017). RNA interference-induced innate immunity, off-target effect, or immune adjuvant? *Front. Immunol.* 8, 331. <https://doi.org/10.3389/fimmu.2017.00331>.
60. Judge, A.D., Bola, G., Lee, A.C., and MacLachlan, I. (2006). Design of noninflammatory synthetic siRNA mediating potent gene silencing in vivo. *Mol. Ther.* 13, 494–505. <https://doi.org/10.1016/j.ymthe.2005.11.002>.
61. Fucini, R.V., Haringsma, H.J., Deng, P., Flanagan, W.M., and Willingham, A.T. (2012). Adenosine modification may be preferred for reducing siRNA immune stimulation. *Nucleic Acid. Ther.* 22, 205–210. <https://doi.org/10.1089/nat.2011.0334>.
62. Judge, A.D., Sood, V., Shaw, J.R., Fang, D., McClintock, K., and MacLachlan, I. (2005). Sequence-dependent stimulation of the mammalian innate immune response by synthetic siRNA. *Nat. Biotechnol.* 23, 457–462. <https://doi.org/10.1038/nbt1081>.
63. Robbins, M., Judge, A., Liang, L., McClintock, K., Yaworski, E., and MacLachlan, I. (2007). 2'-O-methyl-modified RNAs act as TLR7 antagonists. *Mol. Ther.* 15, 1663–1669. <https://doi.org/10.1038/sj.mt.6300240>.
64. Sioud, M., Furset, G., and Cekaite, L. (2007). Suppression of immunostimulatory siRNA-driven innate immune activation by 2'-modified RNAs. *Biochem. Biophys. Res. Commun.* 361, 122–126. <https://doi.org/10.1016/j.bbrc.2007.06.177>.
65. Eberle, F., Giessler, K., Deck, C., Heeg, K., Peter, M., Richert, C., and Dalpke, A.H. (2008). Modifications in small interfering RNA that separate immunostimulation from RNA interference. *J. Immunol.* 180, 3229–3237. <https://doi.org/10.4049/jimmunol.180.5.3229>.
66. Freeman, D.J., McManus, F., Brown, E.A., Cherry, L., Norrie, J., Ramsay, J.E., Clark, P., Walker, I.D., Sattar, N., and Greer, I.A. (2004). Short- and long-term changes in plasma inflammatory markers associated with preeclampsia. *Hypertension* 44, 708–714. <https://doi.org/10.1161/01.HYP.0000143849.67254.ca>.
67. LaMarca, B., Cornelius, D., and Wallace, K. (2013). Elucidating immune mechanisms causing hypertension during pregnancy. *Physiology* 28, 225–233. <https://doi.org/10.1152/physiol.00006.2013>.
68. Rosales, C., Lowell, C.A., Schnoor, M., and Uribe-Querol, E. (2017). Neutrophils: their role in innate and adaptive immunity 2017. *J. Immunol. Res.* 2017, 9748345. <https://doi.org/10.1155/2017/9748345>.
69. (2019). FDA Approves Givosiran for Acute Hepatic Porphyria.
70. Springer, A.D., and Dowdy, S.F. (2018). GalNAc-siRNA conjugates: leading the way for delivery of RNAi therapeutics. *Nucleic Acid Ther.* 28, 109–118. <https://doi.org/10.1089/nat.2018.0736>.
71. Prakash, T.P., Graham, M.J., Yu, J., Carty, R., Low, A., Chappell, A., Schmidt, K., Zhao, C., Aghajan, M., Murray, H.F., et al. (2014). Targeted delivery of antisense oligonucleotides to hepatocytes using triantennary N-acetyl galactosamine improves potency 10-fold in mice. *Nucleic Acids Res.* 42, 8796–8807. <https://doi.org/10.1093/nar/gku531>.
72. Matsuda, S., Keiser, K., Nair, J.K., Charisse, K., Manoharan, R.M., Kretschmer, P., Peng, C.G., VKi, A., Kandasamy, P., Willoughby, J.L., et al. (2015). siRNA conjugates carrying sequentially assembled trivalent N-acetylgalactosamine linked through nucleosides elicit robust gene silencing in vivo in hepatocytes. *ACS Chem. Biol.* 10, 1181–1187. <https://doi.org/10.1021/cb501028c>.
73. Rajeev, K.G., Nair, J.K., Jayaraman, M., Charisse, K., Taneja, N., O'Shea, J., Willoughby, J.L.S., Yucius, K., Nguyen, T., Shulga-Morskaya, S., et al. (2015). Hepatocyte-specific delivery of siRNAs conjugated to novel non-nucleosidic trivalent N-acetylgalactosamine elicits robust gene silencing in vivo. *Chembiochem* 16, 903–908. <https://doi.org/10.1002/cbic.201500023>.
74. Cuellar, T.L., Barnes, D., Nelson, C., Tanguay, J., Yu, S.F., Wen, X., Scales, S.J., Gesch, J., Davis, D., van Brabant Smith, A., et al. (2015). Systematic evaluation of antibody-mediated siRNA delivery using an industrial platform of THIOMAB-siRNA conjugates. *Nucleic Acids Res.* 43, 1189–1203. <https://doi.org/10.1093/nar/gku1362>.
75. Dugal-Tessier, J., Thirumalaairajan, S., and Jain, N. (2021). Antibody-Oligonucleotide conjugates: a twist to antibody-drug conjugates. *J. Clin. Med.* 10. <https://doi.org/10.3390/jcm10040838>.
76. Klabenkova, K., Fokina, A., and Stetsenko, D. (2021). Chemistry of peptide-oligonucleotide conjugates: a review. *Molecules* 26. <https://doi.org/10.3390/molecules26175420>.
77. Muratovska, A., and Eccles, M.R. (2004). Conjugate for efficient delivery of short interfering RNA (siRNA) into mammalian cells. *FEBS Lett.* 558, 63–68. [https://doi.org/10.1016/s0014-5793\(03\)01505-9](https://doi.org/10.1016/s0014-5793(03)01505-9).
78. Chen, C.P., Liu, S.H., Lee, M.Y., and Chen, Y.Y. (2008). Heparan sulfate proteoglycans in the basement membranes of the human placenta and decidua. *Placenta* 29, 309–316. <https://doi.org/10.1016/j.placenta.2008.01.002>.
79. Zhang, M.M., Bahal, R., Rasmussen, T.P., Manautou, J.E., and Zhong, X.B. (2021). The growth of siRNA-based therapeutics: updated clinical studies. *Biochem. Pharmacol.* 189, 114432. <https://doi.org/10.1016/j.bcp.2021.114432>.
80. Shen, W., Liang, X.H., Sun, H., and Crooke, S.T. (2015). 2'-Fluoro-modified phosphorothioate oligonucleotide can cause rapid degradation of P54nrb and PSF. *Nucleic Acids Res.* 43, 4569–4578. <https://doi.org/10.1093/nar/gkv298>.
81. Kirk, B., Jayaprakash, N., Maja, J., Yesseinia, A.-R., Haiyan, P., Christopher, T., Elena, C.-R., Christopher, B., Donald, F., Jeffrey, K., et al. (2021). Expanding the reach of RNAi therapeutics with next generation lipophilic siRNA conjugates. *Nature Portfolio*. <https://doi.org/10.21203/rs.3.rs-946835/v1>.
82. O'Shea, J., Theile, C.S., Das, R., Babu, I.R., Charisse, K., Manoharan, M., Maier, M.A., and Zlatev, I. (2018). An efficient deprotection method for 5'-[O-bis(pivaloyloxy-methyl)]-(E)-vinylphosphonate containing oligonucleotides. *Tetrahedron* 74, 6182–6186. <https://doi.org/10.1016/j.tet.2018.09.008>.
83. Godinho, B.M.D.C., Gilbert, J.W., Haraszti, R.A., Coles, A.H., Biscans, A., Roux, L., Nikan, M., Echeverria, D., Hassler, M., and Khvorova, A. (2017). Pharmacokinetic profiling of conjugated therapeutic oligonucleotides: a high-throughput method based upon serial blood microsampling coupled to peptide nucleic acid hybridization assay. *Nucleic Acid Ther.* 27, 323–334. <https://doi.org/10.1089/nat.2017.0690>.